ACS OMEGA

http://pubs.acs.org/journal/acsodf

Article

Facile and Green Fabrication of Highly Competent Surface-Modified Chlorogenic Acid Silver Nanoparticles: Characterization and Antioxidant and Cancer Chemopreventive Potential

Tamanna Roy, Surya Kanta Dey, Ananya Pradhan, Angsuman Das Chaudhuri, Malay Dolai, Santi M. Mandal, and Sujata Maiti Choudhury*

Cite This: *ACS Omega* 2022, 7, 48018−48033

Read Online

ACCESS | Metrics & More | Article Recommendations

ABSTRACT: The eco-friendly, cost-effective, and green fabrication of nanoparticles is considered a promising area of nanotechnology. Here, we report on the green synthesis and characterization of bovine serum albumin (BSA)-decorated chlorogenic acid silver nanoparticles (AgNPs-CGA-BSA) and the studies undertaken to verify their plausible antioxidant and antineoplastic effects. High-resolution transmission electron microscopy (HR-TEM), dynamic light scattering, X-ray diffraction, and Fourier transform infrared analyses depict an average mean particle size of ∼96 nm, spherical morphology, and nanocrystalline structure of AgNPs-CGA-BSA. DPPH scavenging and inhibition of lipid peroxidation signify the noticeable *in vitro* antioxidant potential of the nanoparticles. The *in vitro* experimental results demonstrate that AgNPs-CGA-BSA shows significant cytotoxicity to Dalton's lymphoma ascites (DLA) cells and generates an enhanced intracellular reactive oxygen species and oxidized glutathione (GSSG) and reduced glutathione (GSH) in DLA cells. Furthermore, mechanism investigation divulges the pivotal role of the downregulated expression of superoxide dismutase (SOD) and catalase (CAT), and these ultimately lead to apoptotic chromatin condensation in AgNPs-CGA-BSA-treated DLA cells. In addition, in vivo experiments reveal an excellent decrease in tumor cell count, an increase in serum GSH and CAT, SOD, and glutathione peroxidase activities, and a decrease in the malondialdehyde (MDA) level in DLA-bearing mice after AgNPs-CGA-BSA treatment. These findings suggest that the newly synthesized biogenic green silver nanoparticles have remarkable *in vitro* antioxidant and antineoplastic efficacy that triggers cytotoxicity, oxidative stress, and chromatin condensation in DLA cells and in vivo anticancer efficacy that enhances the host antioxidant status, and these might open a new path in T-cell lymphoma therapy.

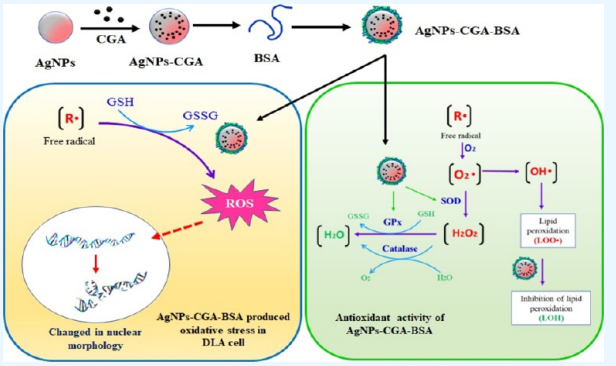

1. INTRODUCTION

Different reactive oxygen species (ROS) are generated as intermediates in the normal process of aerobic metabolism. Free radicals included in ROS oxidize the membrane lipids. As a result, numerous biological components, including lipids, proteins, and DNA, undergo damage.[1] As a result, our bodies are encountered by numerous diseases including diabetes, cancer, atherosclerosis, age-related brain disorders, hemorrhagic shock, cirrhosis, arthritis, and so forth.[2,3] Almost all organisms have highly effective antioxidant defense mechanisms to destroy free radicals. GSH, the most essential hydrophilic antioxidant, safeguards cells against reactive oxygen (ROS) and nitrogen (RNS) species.[4] Among ROS and RNS, the radical forms are eliminated via nonenzymatic reduction with GSH. The removal of hydroperoxides involves enzymatic catalysis by glutathione peroxidase (GPX) and catalase. GSSG, the subsequent oxidized form of GSH, is effectively reduced back to GSH by GSH reductase with the help of NADPH. Essentially, the GSH and GSH-related enzymatic systems are competent tools for detoxification. GSH, being both a nucleophile and a reductant, can undergo reactions with electrophilic or oxidizing species. Glutathione-S-transferases (GSTs), a superfamily of Phase II detoxification enzymes, can cause the conjugation of GSH with electrophilic compounds. For the direct scavenge of radical species, the thiol moiety of GSH is so essential to exert its antioxidant function. The radical chain reactions are blocked by superoxide dismutase (SOD) in rapport with catalase or GPX that

Received: September 15, 2022
Accepted: November 24, 2022
Published: December 12, 2022

https://doi.org/10.1021/acsomega.2c05989
ACS Omega 2022, 7, 48018−48033

regulates the completely free radical scavenging.[5] Enzymatic antioxidants, in particular, often demonstrate their antioxidant activity by breaking down ROS into harmless or neutral chemicals.[6] Numerous dietary antioxidants, such as vitamin E, carotenoids, ascorbic acid, and polyphenols, also exhibit oxidative stress-protective pathways.[7,8] Currently, using a combination of herbs to build a treatment that lowers oxidative stress is possible,[9,10] and various herbal substances have various antioxidant benefits.[11] Therefore, the natural antioxidants derived from food or plant sources and byproducts of food processing are getting a lot of attention today.[12−14] Cancer is a deadly disease triggered by mutated genes, environmental influences, and disrupted cell-regulatory proteins. The incidence of cancer has been increasing in current decades and is one of the major health concerns of the 21st century. GLOBOCAN data for 2020 clearly declared that the cancer incidence has been augmented to 19.29 million, and around 9.95 million cancer deaths have occurred.[15,16] Presently, cancers are treated by surgery, chemotherapy, radiotherapy, hormonal therapy, immunotherapy, transplantation, and other targeted therapies. Phytochemicals or their derived compounds are being increasingly recognized as potent complementary treatments for cancer.[17]

Lymphoma is the largest category of blood cancer, involving the lymphocytes. In India, the incidence of lymphoma is on the expansion. Clonal tumors of immature or mature T lymphocytes at numerous stages of differentiation are termed T-cell lymphomas. Dalton's lymphoma is a transplantable T-cell lymphoma and is spontaneously formed in the thymus of the murine host. Dalton's lymphoma is extensively used as an excellent and interesting model for cancer research, due to its effectiveness in the preclinical system for assessing new or known drugs in various cancer treatments.[18]

According to IUPAC guidelines,[19] chlorogenic acid (CGA, 3-CQA), the most prevalent isomer of caffeoylquinic acid (3-, 4-, and 5-CQA), is currently recognized as 5-CQA. It is a naturally occurring polyphenolic antioxidant that is found in a variety of foods such as coffee, tea, apples, pears, berries, sweet potatoes, lettuce, spinach, beans, and so forth. CGA exhibits antibacterial, anti-inflammatory, anticancer, anti-ulcerogenic, and antidiabetic properties, and in spite of these, to maximize its efficacy, the best delivery systems are crucial.[20,21]

The use of nanoparticles in biomedical fields is made easier by nanobiotechnology. Noble metal nanoparticles such as silver, gold, copper, zinc, titanium, platinum, and magnesium nanoparticles have gained substantial consideration for biomedical applications for their multifunctional theranostic capabilities.[22] Nanomaterials, having high antioxidant properties, offer the intriguing possibility of creating novel therapies with enhanced and focused effects. Silver, gold, and selenium nanoparticles have been proven to have the capacity to suppress oxidative stress due to their effective redox-active radical-scavenging qualities.[23−25] For their advantageous antibacterial, anti-diabetic, anti-oxidative,[26] cytotoxic, and anticancer properties, silver nanoparticles (AgNPs) stand out among metal nanoparticles,[27] and green-synthesized AgNPs are biocompatible and safe for therapeutic applications.[28−30] Today, research is focused on the green fabrication of nanoparticles using herbs or phytocompounds.[31]

Surface coating and modification of metal nanoparticles with a variety of biocompatible and biodegradable materials are becoming more crucial for achieving their desired stability.[32] Proteins are eye-catching materials for surface modification because of their high adsorption capability, biodegradability, and low toxicity. Albumin has generally been extensively used as a suitable carrier of anticancer medicines for its exceptional biocompatibility, increased blood stability, and tendency to concentrate in inflammatory or malignant tissues.[33] Due to its good biodegradability, nontoxicity, higher bioavailability, better chemical stability, and long half-life, bovine serum albumin (BSA) is widely used in the field of drug delivery.[34]

Some nanoparticles produce ROS[35] and can cause efficient conversion of GSH to GSSG in phosphate-buffered saline and also induce oxidation of GSH in live cells.[36] Therefore, the focus of the current study is to synthesize and characterize surface-modified chlorogenic acid silver nanoparticles (AgNPs-CGA-BSA) and to investigate their *in vitro* antioxidant potential and antineoplastic efficacy against Dalton's lymphoma ascites (DLA). We also examined the in vivo anticancer potential in DLA-bearing Swiss albino mice to detect whether there is any capability of AgNPs-CGA-BSA to enhance the host antioxidant status which can antagonize the cancer ailments.

2. MATERIALS AND METHODS

2.1. Materials. All the chemicals such as methanol, 2,2-diphenyl-1-picrylhydrazyl (DPPH), hydrogen peroxide, phenazine methosulfate (PMS), silver nitrate ($AgNO_3$), sodium nitroprusside, trichloro acetic acid (TCA), trichloro acetic acid (TCA), sodium chloride (NaCl), hydrochloric acid (HCl), sulfosalicyclic acid (SSA), 2,4,4 dithionitrobenzoic acid (DTNB), pyrogallol, hydrogen peroxide (H_2O_2), TrisHCl, potassium dihydrogen phosphate (KH_2PO_4), thio barbaturic acid (TBA), reduced nicotinamide adenine dinucleotide (NADH), Evans blue, taurine, ethylenediaminetetraacetic acid, 2-deoxy-2-ribose, sulfanilamine, naphthylethylenediamine-dihydrochloride, sodium chloride (NaCl), ferric chloride ($FeCl_3$), sulfuric acid (H_2SO_4), 2-deoxy-2-ribose, potassium chloride (KCl), ferrous sulfate (FeSO4), hydrogen peroxide (H_2O_2), ethylene diamine tetra acetic acid (EDTA), nitro blue tetrazolium (NBT), *n*-butanol, pyridine, sodium citrate, citric acid, ascorbic acid, orthophosphoric acid, BSA, ascorbic acid, and other chemicals were purchased from SRL chemicals, India, Merck India, Ltd., Mumbai, India. All chemicals used were of analytical grade. Chlorogenic acid, Histopaque 1077, and 3-(4,5-dimethyl-2-thiazolyl)-2,5-diphenyl-tetrazolium bromide (MTT) were purchased from Sigma-Aldrich Co. LLC, US.

2.2. Synthesis. *2.2.1. Preparation of Colloidal AgNPs by the Conventional Method.* Stock solutions of silver nitrate with a concentration of metal salt ($AgNO_3$, 0.01 M) and trisodium citrate dihydrate (HOC (COONa) (CH_2COONa) $2{\cdot}2H_2O$, 0.01 M) were prepared in a conical flask and stored in the dark to protect against light. Next, 0.01 M sodium borohydride ($NaBH_4$) was prepared as a stock solution. To prepare Sample 1 (S1), 5 mL of 0.01 M trisodium citrate dihydrate was mixed with 5 mL of 0.01 M $AgNO_3$ solution under magnetic stirring for 10 min at room temperature before 0.1 mL of $NaBH_4$ was added. The color of the mixture quickly changed to yellow, indicating the formation of AgNPs.[37]

2.2.2. Preparation of Biogenic AgNPs Using Chlorogenic Acid. First, 100 mL of 1 mM solution of silver nitrate (Merck, India) was prepared. Then, 8 mM chlorogenic acid was added to that during magnetic stirring at 500 rpm with slight heat (40 °C) for 45 min. This setup was incubated in a dark condition to minimize the photoactivation of silver nitrate. After 45 min,

https://doi.org/10.1021/acsomega.2c05989
ACS Omega 2022, 7, 48018−48033

a color change is observed, which indicates the initiation of biogenic nanoparticle (AgNPs-CGA) synthesis.[38]

2.2.3. Modification of Biogenic AgNPs-CGA by BSA. The surface of the produced AgNPs-CGA is modified using a BSA solution. First, 100 mL of AgNPs-CGA was mixed with 30 mL of a readymade BSA solution (1.5 mg/mL) and left overnight at room temperature and 440 rpm magnetic stirring in the dark. It turned a mild shade of yellow and was centrifuged for 30 min at 12,000 rpm. The nanoparticles were vacuum-dried, and the supernatant was removed. To prevent BSA degradation, the produced BSA-modified biogenic nanoparticles (AgNPs-CGA-BSA) were stored in a chilled environment.[39]

2.3. Physiochemical Characterization of AgNPs-CGA-BSA. The average hydrodynamic particle diameter and polydispersity index (PDI) were examined by the Zetasizer Nano ZS instrument (ZEN 3600, Malvern Instruments, UK) at a constant temperature of 25 ± 1 °C.[40] The zeta potential was measured at 25 °C. The PDI was assessed for the particle size distribution.

The absorbance spectrum of the colloidal AgNPs, AgNPs-CGA, and AgNPs-CGA-BSA samples was obtained in the range of 200−850 nm, using a UV−vis spectrometer (UV-1800 Shimadzu, Japan).[41]

Fourier transform infrared (FTIR) measurements were detected in the samples and were used for capping and efficient stabilization of the AgNPs, AgNPs-CGA, and AgNPs-CGA-BSA, separately, with an FTIR system using a Perkin Elmer Spectrum Express Version 1.03.00. The powdered sample was mixed with KBr for the preparation of pellets, and its FTIR spectra were observed using an FTIR spectroscope at a wavelength of 4000 to 400 cm^{-1} with an accuracy of ±0.01 cm^{-1} and resolution of 4 cm^{-1}.[42]

The X-ray diffraction (XRD) measurements were carried out using an X-ray diffractometer (Model PW 1710). For crystalline samples, an operating voltage was set to 30 kV at a wavelength of 0.154 nm (Cu Kα), and the operating current was adjusted to 40 mA and 2θ = 20−70°.[40] The identification of AgNPs, AgNPs-CGA, and AgNPs-CGA-BSA was analyzed by matching the peak positions of XRD patterns with the patterns of the JCPDS (Joint Committee on Powder Diffraction Standards) database.

HR-TEM study was carried out to evaluate the morphological character of AgNPs-CGA and AgNPs-CGA-BSA separately by CM12 PHILIPS. For this, AgNPs-CGA-BSA was prepared in Milli-Q water, and freshly prepared AgNPs-CGA-BSA suspensions were placed onto a carbon-coated copper grid as a thin liquid film by a dropping method.[43,44]

2.4. Stability Study. The stability of AgNPs-CGA-BSA was assessed using UV−vis absorption spectra at several concentrations, time intervals, and pH values. The measurements were performed in a triplicate manner.[45]

2.5. Study on *In Vitro* Antioxidant Activity. *2.5.1. DPPH Scavenging Assay.* DPPH is an unchanging free radical, due to the delocalization of the spare electron on the whole substances. In brief, 2.8 mL of AgNPs-CGA-BSA with different concentrations (50, 100, 250, and 500 μg/mL) was mixed with 0.2 mL of 1,1-diphenyl-2-picrylhydrazine (DPPH) (100 μM in methanol) and standard ascorbic acid (10−200 μg/mL in methanol). The mixture was placed at room temperature. Then, the reaction mixture was incubated at 37 °C for 30 min under dark conditions. After incubation, the absorbance of the reaction mixture was measured using a spectrometer (ShimadzuU-245) at 517 nm. The DPPH radical scavenging activity of AgNPs-CGA-BSA was computed using the following formula.[46]

$$\text{Percentage inhibition} = \frac{C - T}{C} \times 100 \quad (1)$$

where C = absorbance of the control and T = absorbance of the test sample.

2.5.2. Lipid Peroxidation Scavenging Assay. At first, young adult Swiss albino mice liver was separated and homogenized with an ice-cold Tris−HCl buffer (20 mM, pH 7.4) to produce a 1/10 homogenate and centrifuged at 12,000 rpm at 4 °C for 15 min. Then, 1 mL of the supernatant was mixed with various concentrations (50, 100, 250, and 500 μg/mL) of AgNPs-CGA-BSA and also mixed with 30 mM KCl, 0.16 mM $FeSO_4$, and 0.06 mM ascorbic acid and incubated at 37 °C for 1 h for reaction. After incubation, the reaction mixture was finished by adding 1.0 mL of TCA (10% w/v) and 1.5 mL of TBA (1% w/v), and the net volume was made up to 4 mL by mixing distilled water and keeping it in a water bath for 30 min. After the water bath condition, the reaction mixture was cooled. Then, this reaction mixture was added with 1 mL of distilled water and 5 mL of *n*-butane/pyridine (15:1 v/v). Finally, this mixture was centrifuged at 4000 rpm for 10 min. The absorbance of the mixture was measured at 532 nm.[47] The percentage inhibition was determined using the previously mentioned formula (eq 1). Identical tubes were kept in the dark and served as blanks. The results were expressed in percent inhibition as compared to the control.

2.6. Study on *In Vitro* Anticancer Activity against DLA Cells. *2.6.1. Animal Maintenance and Maintenance of DLA Cell Line.* Female Swiss albino mice, 8−10 week old (each having a weight of 18−25 g), were housed in wire cages (45 × 45 × 50 cm) in a humidity- and temperature-controlled room (22 ± 2 °C). The light was provided for 14 h per day. Standard feed and water were supplied ad libitum.[48] After 10 days of acclimatization, mice were randomly divided into different groups for scheduled experiments. DLA cells were procured from Chittaranjan National Cancer Research Institute (CNCI), Kolkata. The DLA cell line was maintained by weekly intraperitoneal transplantation in the female Swiss albino mice at a concentration of 2 × 10^6/cells per mouse. Washed DLA cells free from contaminating RBC were cultured in RPMI-1640 medium supplemented with 10% FBS and antibiotic solution (100 U mL^{-1} penicillin, 10 mg/mL, streptomycin, and 4 mM L-glutamine) under a 5% CO_2 and 95% humidified atmosphere at 37 °C in a CO_2 incubator. Viable cells were grown in an exponential form until it reaches 1 × 10^6 cells/mL growth and used for different experiments.[40] According to the guidelines of the Institutional Animal Ethical Committee under the regulations of the Committee for Control and Supervision of Experiments on Animals (CPCSEA), all experiments were carried out (approval no. VU/IAEC-I/SMC-1/3−10/19-dt-11/12/19).

2.6.2. Isolation of Mice Lymphocyte Cells. Blood was taken from healthy albino mice and kept in heparin-coated vacutainers.[40] The blood sample was taken with the addition of Histopaque and centrifuged at 2000 rpm for 20 min at room temperature. The lymphocyte monolayer was transferred into an autoclaved centrifuge tube and washed with phosphate buffer solution (pH 7.4). Then, mice lymphocyte cells (MLCs) were suspended in an RPMI medium supplemented with 10% FBS and incubated in a CO_2 incubator for 24 h at 37 °C.

https://doi.org/10.1021/acsomega.2c05989
ACS Omega 2022, 7, 48018−48033

2.6.3. Cytotoxicity Study by MTT Assay. The cytotoxicity of AgNPs, AgNPs-CGA, and AgNPs-CGA-BSA on MLCs and DLA cells was determined by MTT assay.[40] At first, cells (1×10^6/well) were plated in 100 μl of the medium and treated with different concentrations (0.5, 1, 5, 10, and 25 μg/mL) of CGA, AgNPs, AgNPs-CGA, and AgNPs-CGA-BSA, respectively, except the control cells and incubated for 24 h at 37 °C. After removal of the treated drugs, the cells were washed with PBS (pH 7.4), and 5 mg/mL 0.5% MTT in phosphate-buffered saline solution was added to each well. After 3 h of incubation, 0.1% DMSO was added to each well to dissolve formazan crystals. Then, the absorbance was recorded at 540 nm, using an ELISA analyzer (Bio-Rad, model 680). The cell viability percentage was calculated concerning untreated cells.[41]

2.6.4. Determination of Intracellular ROS Generation in DLA Cells. In brief, DLA cells were exposed to AgNPs, AgNPs-CGA, and AgNPs-CGA-BSA at 5 μg/mL for 24 h. After treatment, the cells were washed with phosphate buffer, followed by incubation with 1 μg/mL 2′,7′-dichlorodihydro fluorescein diacetate (H_2DCFDA) for 30 min at 37 °C. The cells were again washed three times with fresh culture media. At 485 nm excitation and 520 nm emission, DCF fluorescence was determined using a Hitachi F-7000 fluorescence spectrophotometer and was also observed by fluorescence microscopy (LEICA DFC295, Germany).[40]

2.6.5. Estimation of GSH and GSSG in DLA Cells. At first, 0.2 mL of each sample was lysed and mixed with 4% sulfosalicylic acid, and centrifugation was carried out to settle the precipitated proteins. The supernatant was aspirated, and then, 2 mL of 0.6 mM DTNB was added and allowed to remain for 10 min. Then, the optical density of the yellow-colored complex formed by the reaction of GSH and DTNB was measured at 412−420 nm. A standard curve was calculated with standard reduced glutathione (GSH). GSH content was expressed as μg of GSH mg^{-1} protein. All experiments were executed in triplicate. The oxidized glutathione level was measured after the derivatization of GSH with 2-vinyl pyridine. In brief, with 0.1 mL of the sample, 2 μL of 2-vinyl pyridine was added and incubated for 1 h at 37 °C. The mixture was then mixed with 4% sulfosalicylic acid and was centrifuged to settle the precipitated proteins. The GSSG level was estimated after the reaction of DTNB with the aspirated supernatant at 412 nm.[40] The levels of GSSG were expressed as μg of GSSG mg^{-1} protein.

2.6.6. Western Blotting of Enzymatic Antioxidants (SOD and CAT) in DLA Cells. AgNPs-CGA-BSA (at IC_{50} dose from MTT assay)-treated DLA cells (1×10^6 cells mL^{-1}) were exposed to RIPA buffer, supplemented with the cocktail protease inhibitor. The total protein was separated by sodium dodecyl sulfate-polyacrylamide electrophoretic gel electrophoresis and transferred into PVDF membranes. The membranes were stained with Coomassie blue for 10 min. The membranes were then preincubated in a blocking buffer (pH 8) for 2 h on a rocker at room temperature. After probing with respective primary antibodies at 4 °C, the membranes were washed thrice in TBST. Then, the PVDF membranes were incubated at 37 °C for 1 h with ALP-conjugated suitable secondary antibodies (1:10,000) against the primary antibodies. After that, the membranes were washed three times in TBST, stained with NBT-BCIP buffer, and kept in a dark room for 15 min. The band for SOD and CAT was visualized by Gel Doc, and the pictures were captured. Densitometry of the appropriately sized bands was carried out using Image J 148-JDK 6 software.[49,50]

2.6.7. Apoptotic Changes in Chromatin by DAPI and PI Staining. DLA cells (1×10^6 cells mL^{-1}) were seeded in a Petri plate, incubated for 24 h at 37 °C and 5% CO_2, and then fixed with 70% ethanol at −20 °C for 2 h. After fixation, treated cells were washed and stained with 2′,6′-diamidino-2-phenylindole dihydrochloride (DAPI) (1 μg/mL) at 37 °C for 5 min and RNAse−propidium iodide (PI) mixture (1 mg/mL) at 37 °C for 15 min.[40] The cells were washed with phosphate buffer and examined under the fluorescence microscope.

2.7. Study of In Vivo Anticancer Effects in DLA-Bearing Swiss Albino Mice. *2.7.1. Treatment Schedule.* Fifty-four female Swiss albino mice were divided into nine groups (n = 6, weight = 25−30 g).

2.7.2. Animal Group Administrated Drug.

Group I: 0.9% NaCl (saline control)
Group II: DLA control (1×10^6 cells/mL per mouse)
Group III: DLA + CGA (25 mg/kg body weight)
Group IV: DLA + CGA (50 mg/kg body weight)
Group V: LA+AgNPs-CGA (2.5 mg/kg body weight)
Group VI: LA+AgNPs-CGA (5 mg/kg body weight)
Group VII: DLA+AgNPs-CGA-BSA (0.5 mg/kg body weight)
Group VIII: LA+AgNPs-CGA-BSA (1 mg/kg body weight)
Group IX: DLA + 5-FU (20 mg/kg body weight)

All groups received 0.1 mL of 1×10^6 DLA cells/mouse intraperitoneally except Group I (saline control). This was considered "day zero". Group II served as the DLA control. After 24 h of tumor inoculation, Groups III, IV, V, VI, VII, and VIII received above-said test samples and Group IX received reference standard drug 5-FU (20 mg/kg body weight) once daily for 14 consecutive days. Then, the animals were sacrificed by cervical dislocation. Tumor volume was measured. For the study of hepatic and renal oxidative stress parameters [GSH, malondialdehyde (MDA), CAT, SOD, GST, and GPX], liver and kidney tissue was collected.

2.7.3. Measurement of Tumor Cell Count in DLA-Bearing Swiss Albino Mice. During the time of sacrifice, 2 mL of normal saline was injected intraperitoneally into each mouse. Then, the ascitic fluid was drawn aseptically from the peritoneal cavity of every mouse. The fluid was taken in a WBC pipette and diluted 100 times with phosphate-buffered saline. Then, a drop of the diluted cell suspension was charged on the Neubauer counting chamber, and the number of tumor cells was counted.[51]

2.7.4. Hematological Analysis. Sterile syringes (5 mL) were used to collect blood samples from all DLA-bearing mice. For the examination of potential hematologic toxicity, whole blood was taken in an EDTA-coated sterile container. The total count of WBC, RBC, and hemoglobin percentage was measured for hematological analysis.[52]

2.7.5. Histopathologic Analysis. From sacrificed animals of all groups, livers and kidneys were collected. The collected organs were fixed in 10% neutral buffered formalin. The tissues were then dehydrated in graded alcohols, and paraffin embedding was carried out. Then, the tissue sections were stained with hematoxylin and eosin and observed under a light microscope, and photomicrographs were taken.[53]

2.8. Measurement of the In Vivo Host Antioxidant Status in DLA-Bearing Swiss Albino Mice. *2.8.1. Estima-*

https://doi.org/10.1021/acsomega.2c05989
ACS Omega 2022, 7, 48018−48033

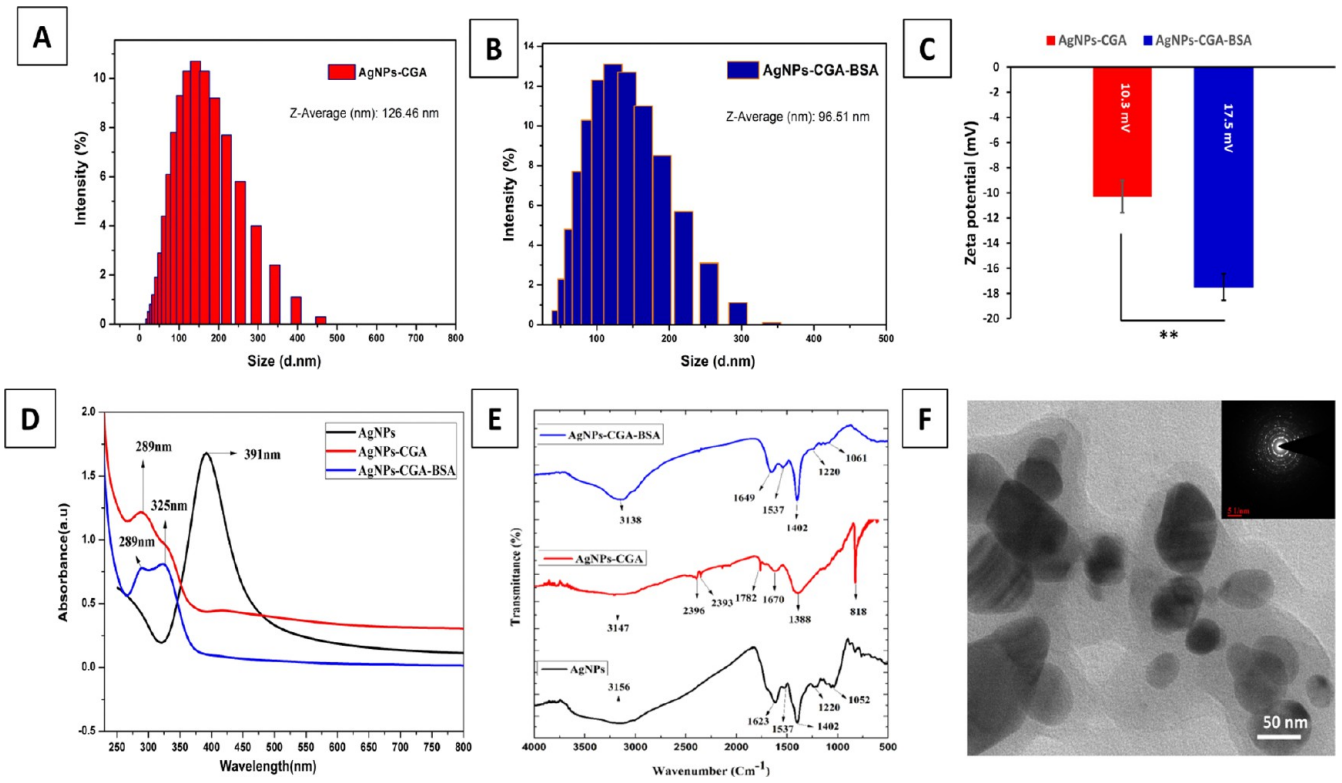

Figure 1. Chemical characterizations and morphological analysis of CGA, AgNPs-CGA, and AgNPs-CGA-BSA. The hydrodynamic diameters of AgNPs-CGA (126.5 ± 0.288 nm) and AgNPs-CGA-BSA (96.51 ± 0.005 nm) were measured by dynamic light scattering (A,B); surface zeta potential of AgNPs-CGA and AgNPs-CGA-BSA (C); UV−vis absorption spectrum analysis of AgNPs, AgNPs-CGA, and AgNPs-CGA-BSA (D); Fourier transform infrared spectroscopy (FTIR) analysis of AgNPs, AgNPs-CGA, and AgNPs-CGA-BSA (E); and TEM images of AgNPs-CGA-BSA; scale bar: 50 nm (F).

tion of the GSH Level of Mice Liver and Kidney. Reduced glutathione (GSH) was estimated using the Griffith method[51] with modifications. Briefly, the reaction mixture consisted of 200 μL of tissue homogenate and 100 μL of sulfosalicylic acid. Then, this mixture was centrifuged at 3000 rpm for 10 min at 4 °C. The supernatant was taken, and 1.8 mL of DTNB was mixed with it and shaken well. The absorbance was measured at 412 nm using a UV−vis spectrophotometer.

2.8.2. Determination of Hepatic and Renal MDA Levels. MDA assay was measured by the method of Ohkawa with some modifications. Briefly, 1 mL of homogenate tissue, 0.2 mL of 8.1% sodium dodecyl sulfate, 1.5 mL of acetate buffer (20% pH 3.5), and 1.5 mL of an aqueous solution of thiobarbituric acid (TBA) (0.8%) were vigorously mixed in a test tube. Then, the mixture was heated at 95 °C for 60 min. After heating, a red pigment was produced, and that was extracted with 5 mL of the *n*-butanol−pyridine mixture and centrifuged at 5000 rpm for 10 min at room temperature.[54] The absorbance of the supernatant was noted at 535 nm.

2.8.3. Estimation of the Catalase (CAT) Level of Mice Liver and Kidney. Catalase was estimated by the method of Aebi.[55] The reaction mixture contained 0.1 mL of tissue homogenate and 1.9 mL of 15 mM PBS. The reaction was initiated by adding 1 mL of 30 mM H_2O_2. The decrease in absorbance at 240 nm was observed for 2 min.

2.8.4. Determination of the Hepatic and Renal SOD Level. The SOD activity of the supernatant was estimated[51] by determining the percentage of inhibition of the pyrogallol auto-oxidation by SOD. Initially, 2 mL of the buffer mixture (50 mM Tris HCl and 10 mM hydrochloric acid in the presence of 1 mM EDTA), 100 μL of 2 mM pyrogallol, and 10 μL of tissue homogenate were taken and mixed vigorously. The absorbance of the supernatant was measured in the spectrophotometer (UV-245 Shimadzu, Japan) at 420 nm for 3 min.

2.8.5. Estimation of the Glutathione-S-Transferase (GST) Level in the Liver and Kidney. Glutathione-S-transferase (GST) activity was estimated.[56] The reaction mixture consists of 0.1 mL of tissue homogenate, 0.2 mL of 100 mM PBS, 0.05 mL of 1 mM GSH, and 0.02 mL of 60 mM 1-chloro-2,4 dinitrobenzene (CDNB) in a test tube. The mixture was poured sincerely into a cuvette. Finally, the absorbance was measured at 340 nm. The enzyme activity was expressed as the recorded data were expressed as units/mg protein.

2.8.6. Determination of Hepatic and Renal Glutathione Peroxidase (GP_X). Glutathione peroxidase was assayed by the method. The reaction mixture consists of 0.2 mL of liver and kidney homogenate, 0.1 mL of 2.5 mM H_2O_2, 0.2 mL of 0.4 M sodium phosphate buffer, 0.1 mL of 10 mM sodium azide, and 0.2 mL of 4 mM GSH. Then, the reaction mixture was incubated for 5 min at 37 °C. To stop the reaction, 0.4 mL of 10% TCA was added and centrifuged for 20 min at 3200 rpm. Then, in 0.5 mL of the supernatant, 1 mL of 5,5′-dithiobisnitrobenzoic acid (DTNB) and 3 mL of disodium hydrogen phosphate (Na_2HPO_4) were mixed. The absorbance was measured at 420 nm.[57]

2.9. Statistical Analysis. All analyses were run in triplicate and expressed as means ± standard deviation (SD). Mean values between the groups in biochemical analyses were considered significantly different at the $p < 0.05$ confidence level, after the performance of the ANOVA single/double

https://doi.org/10.1021/acsomega.2c05989
ACS Omega 2022, 7, 48018−48033

Scheme 1. Graphical Representation of the Mechanism of Synthesis of AgNPs, AgNPs-CGA, and AgNPs-CGA-BSA. (Photographs are created by the author, S.K. Dey Copyright 2022.)

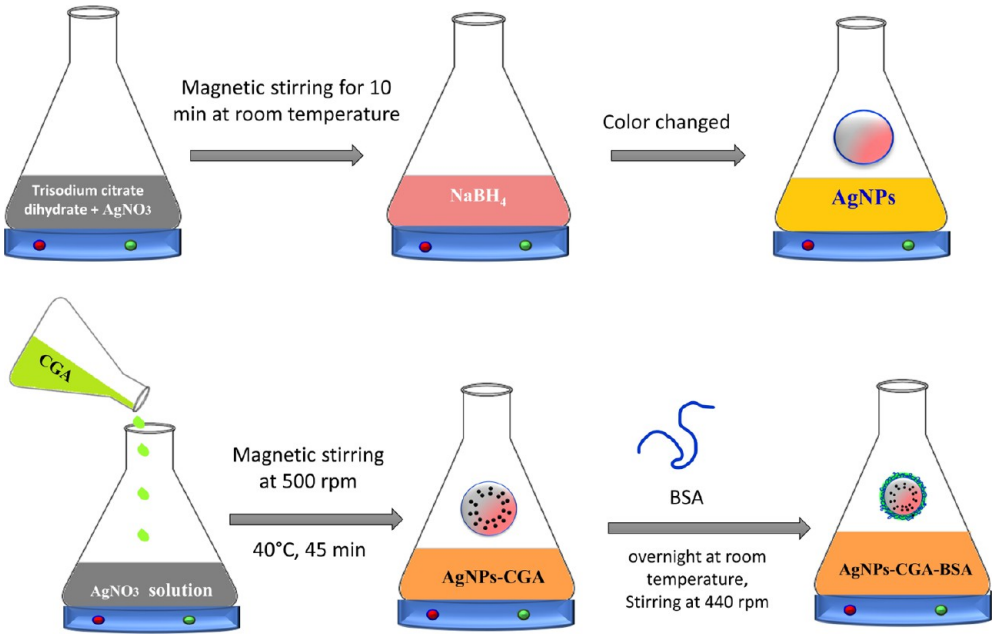

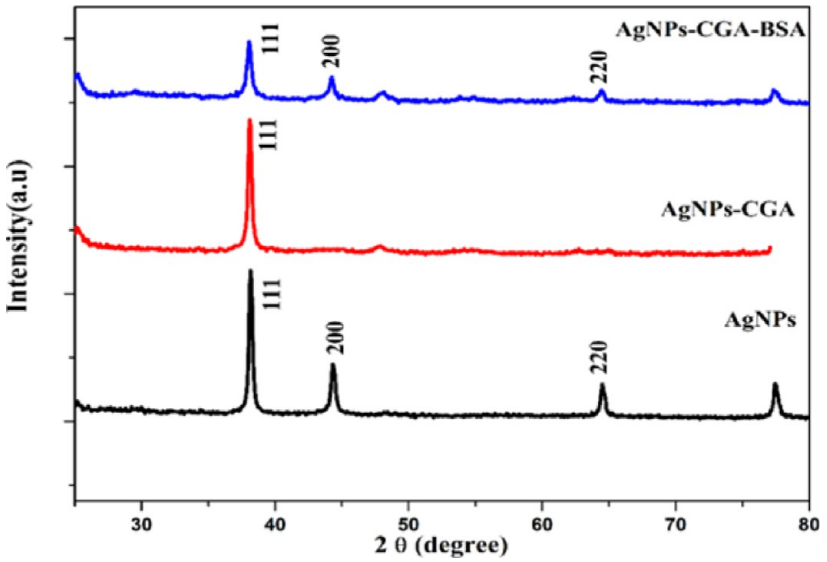

Figure 2. XRD study of AgNPs, AgNPs-CGA, and AgNPs-CGA-BSA.

factor statistical analysis followed by the student's *t*-test using Origin software (Origin Lab, USA).

3. RESULTS AND DISCUSSION

3.1. Characterization. The size of AgNPs-CGA and AgNPs-CGA-BSA was found to be 126.5 and 96.51 nm, respectively, with a respective PDI of 0.270 and 0.265 (Figure 1A,B). The zeta potential measurement showed that AgNPs-CGA and AgNPs-CGA-BSA possess negative zeta potentials of −10.3 and −17.5 Mv (Figure 1C), respectively. The negative surface charge may be due to the aggregation of silver metal on the surface of these nanoparticles.[58] UV−vis spectroscopy is a very steadfast technique to screen the formation and stability of AgNPs.[59] The color change during the formation of metal nanoparticles was for the surface plasmon resonance phenomenon. Free electrons of metal nanoparticles give rise to the surface plasmon resonance absorption band that is produced due to the combined vibration of metal NP electrons with a light wave. The sharp bands of nanoparticles were observed at 391, 289, and 289−325 nm (Figure 1D) in the case of AgNPs, AgNPs-CGA, and AgNPs-CGA-BSA, respectively.[60] The peak originates from the excitation of electrons of AgNPs-CGA-BSA induced by the electromagnetic field which would enhance the rate of reduction of metal ions.

FTIR spectra of standard chlorogenic acid show bands that are well-correlated to 3300, 1686, 1640, and 1526 cm^{-1} corresponding to O−H, C═O, and C−H, stretching (Figure 1E). AgNPs show bands that are well-correlated to 1052, 1220, 1537, 1623, and 3156 cm^{-1} corresponding to C−Cl, C−F, C−H, C═O, and N−H stretching, respectively. AgNPs-CGA shows bands that show 1670, 2393, 2396, 3147, 1782, and 818 cm^{-1} corresponding to C═O, Si−H, P−H, N−H, N−H, C═

https://doi.org/10.1021/acsomega.2c05989
ACS Omega 2022, 7, 48018−48033

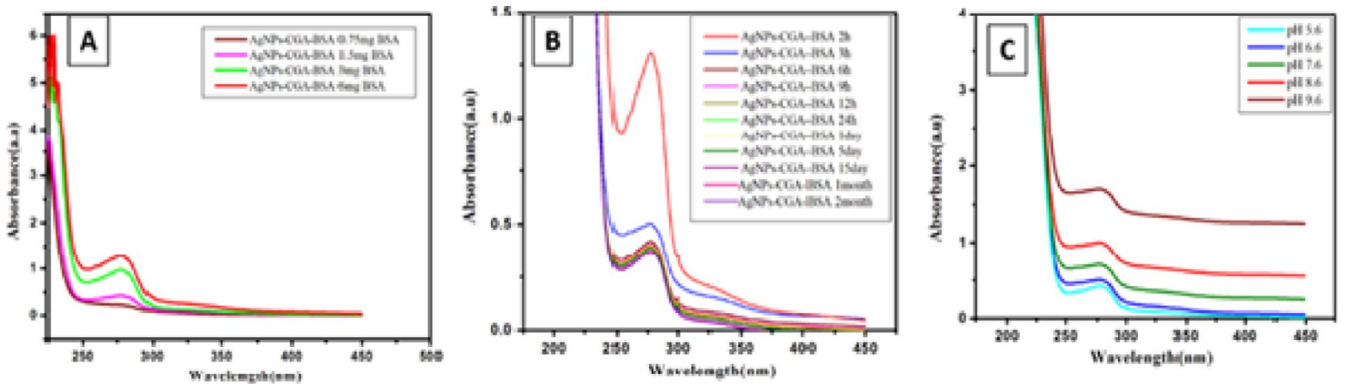

Figure 3. Stability study of AgNPs-CGA-BSA. (A) UV−vis absorption spectra of AgNPs-CGA-BSA at different concentrations of AgNPs-CGA-BSA; (B) UV−vis absorption spectra of AgNPs-CGA-BSA at different time intervals; and (c) UV−vis absorption spectra of AgNPs-CGA-BSA at different pH values.

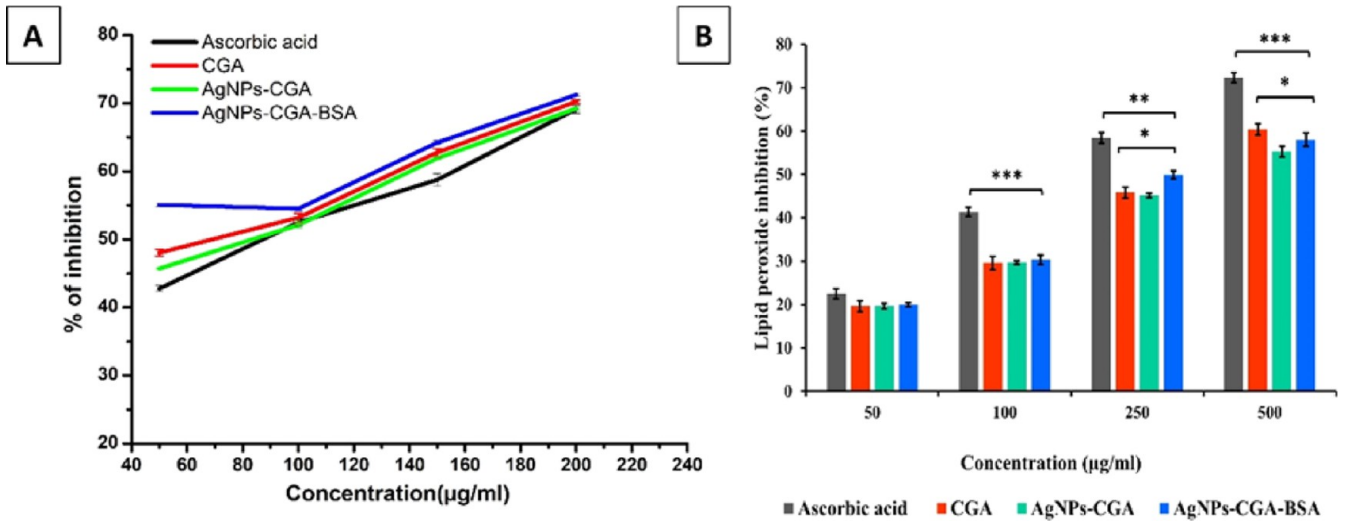

Figure 4. *In vitro* antioxidant activity: *in vitro* 1,1-diphenyl-2-picrylhydrazine (DPPH) scavenging assay of CGA, AgNPs-CGA, and AgNPs-CGA-BSA (A) and inhibition of lipid peroxidation of CGA, AgNPs-CGA, and AgNPs-CGA-BSA (B). Ascorbic acid was used as a standard antioxidant agent. Results are expressed as mean ± SEM, $n = 3$; (*$p < 0.05$, **$p < 0.01$, and ***$p < 0.001$).

O, and C−H stretching. AgNPs-CGA-BSA shows 3138, 1649, 1537, 1402, 1248, and 1061 cm^{-1} corresponding to N−H, C═O, C═O, C═C, C−H, C−F, and C−Cl stretching. FTIR spectroscopy showed lesser stretching in AgNPs-CGA-BSA. CGA contains hydroxyl groups in its structure, which produces the characteristic fingerprint region of O−H stretching vibrations at 3138 cm^{-1}.[61−65]

The average mean particle sizes of AgNPs-CGA and AgNPs-CGA-BSA were 96 ± 2.081 and 50.5 ± 0.288 nm, respectively (Figure 1F). A hydrated layer in the transmission electron microscopy (TEM) image consists of a swollen phytochemical capping on the surface of the nanoparticles.[66−69] The nanoparticles were morphologically spherical and consist of a nanocrystalline structure.[40]

Synthesized and air-dried AgNPs, AgNPs-CGA, and AgNPs-CGA-BSA are shown in Scheme 1. A number of Bragg reflections were detected with 2θ values of 38.04, 44.31, and 64.49° that correspond to the lattice plane (111), (200), and (220) facets of silver, respectively. The XRD pattern showed the distinct diffraction patterns of the powdered sample, and it signified that they were crystalline and the peak co-ordination was quite well with the Powder Diffraction Standard (JCPDS) cards of the Joint Committee for the respective metal (Figure 2).[11]

3.2. Stability Study. Stability is an essential criterion for nanoparticle-based applications. The stability of AgNPs-CGA-BSA was analyzed against various concentrations, time intervals, and different pH values. The stability of AgNPs-CGA-BSA was the highest at pH 7.6. AgNPs-CGA-BSA was more stable under refrigeration. The stability study of biogenic AgNPs-CGA-BSA demonstrated that the absorption wavelength and color of the nanoparticle solution hardly changed during 2 months (Figure 3).[70]

3.3. *In Vitro* Antioxidant Activity. *3.3.1. DPPH Assay.* DPPH is a stable free radical which is nitrogen-centered, and upon reduction, its violet color is changed to yellow by the process of proton or electron donation. The compounds that can perform this reaction can be considered radical scavengers and therefore are antioxidants.[71] The results showed the percentage of DPPH radical scavenging activity of ascorbic acid, CGA, AgNPs-CGA, and AgNPs-CGA-BSA separately (different concentrations) (Figure 4A). IC_{50} values of ascorbic acid, CGA, AgNPs-CGA, and AgNPs-CGA-BSA are 95.31, 94.03, 95.93, and 91.72 μg/mL, respectively (Table 1). DPPH scavenging activity was found to be higher after AgNPs-CGA-

https://doi.org/10.1021/acsomega.2c05989
ACS Omega 2022, 7, 48018−48033

Table 1. Antioxidant Activity of CGA, AgNPs-CGA, and AgNPs-CGA-BSA with Their Respective IC_{50} Values[a]

	IC_{50} values (μg/mL)	
test samples	DPPH (%)	lipid peroxidation scavenging (%)
ascorbic acid	95.31 ± 0.081	128.38 ± 0.004
CGA	94.03 ± 0.008	165.53 ± 0.040
AgNPs-CGA	95.93 ± 0.004	180.89 ± 0.085**
AgNPs-CGA-BSA	91.72 ± 0.004*	172.41 ± 0.004*

[a]Ascorbic acid was used as a standard drug. Results are expressed as mean ± SEM. n = 3; *p < 0.05; **p < 0.01; compared with CGA.

BSA treatment, exhibiting consistently higher activity than ascorbic acid, CGA, and AgNPs-CGA in all concentrations. Based on the results obtained from this study, it may be said that AgNPs-CGA-BSA is a very powerful free radical inhibitor or scavenger, as well as a primary antioxidant that reacts with free radicals, which may limit free radical damage occurring in the human system. The effects of an antioxidant on DPPH scavenging activity happened due to its hydrogen-donating activity.

3.3.2. Lipid Peroxidation Scavenging Assay. Lipid peroxidation occurs at polyunsaturated fatty acids present in the membrane lipid bilayer. It undergoes oxidation, resulting in the formation of malonaldehyde (MDA) which reacts with two molecules of TBA to form TBARS, a pinkish-rendering.[72] The percentage of lipid peroxidation scavenging of the above-said different molecules is depicted in Figure 4B. The percentage of lipid peroxidation scavenging was increased in a concentration-dependent manner, and AgNPs-CGA-BSA significantly inhibited lipid peroxidation with an IC_{50} value of 172.41 μg/mL compared to CGA (IC_{50} = 165.53 μg/mL), as shown in Table 1.

3.4. *In Vitro* Antineoplastic Activity. *3.4.1. In Vitro Cell Viability of DLA Cells.* The effect of AgNPs, CGA, AgNPs-CGA, and AgNPs-CGA-BSA on viability was examined using the MTT assay. Results showed that AgNPs-CGA-BSA was able to reduce DLA cell viability significantly in a dose-dependent manner compared to CGA (Figure 5A). This cell-killing ability indicates the potent cytotoxic efficacy of AgNPs-CGA-BSA against DLA cells. The IC_{50} values of AgNPs, CGA, AgNPs-CGA, and AgNPs-CGA-BSA were found to be 4.78, 6.29, 5.73, and 2.5 μg/mL respectively, whereas no significant toxic effect was observed in MLCs in AgNPs-CGA-BSA-treated groups. AgNPs exhibited a significant toxic effect in MLC cells compared to other groups (Figure 5B). The study suggested that AgNPs-CGA-BSA has a potent cytotoxic effect against DLA cells without producing toxic effects in MLC cells. These results may be helpful to use AgNPs-CGA-BSA as an anticancer agent in cancer therapy.[73]

3.4.2. Intracellular ROS Generation in DLA Cells. ROS can promote abnormal cell signaling, oxidative cell damage, apoptosis, and several pathophysiological conditions.[74,75] Treatment of AgNPs-CGA and AgNPs-CGA-BSA for 24 h induced intracellular ROS generation as induced by DCF fluorescence intensity in DLA cells (Figure 6A,B), and also, a significant increase in ROS levels was observed by fluorescence spectrophotometry, which indicated oxidative-stress-induced pathophysiological conditions in DLA cells.

3.4.3. Intracellular Glutathione Level. GSH acts as an important intracellular reducing agent due to the thiol groups. In the physiological environment, glutathione is converted to its oxidized form, disulfide-linked dimeric form GSSG, and it maintained redox homeostasis.[40] Our present study showed that GSH levels in DLA cells were significantly decreased by AgNPs-CGA-BSA, whereas GSSG levels were significantly increased (Figure 7). The lower level of GSH indicates the effective conversion of GSH to its oxidized state of GSSG as a result of ROS generation induced by AgNPs-CGA-BSA.

Most of the tumor tissues have incomplete vascular remodeling with a gap of 10−1000 nm due to uncontrolled growth and metabolism. AgNPs-CGA-BSA can reach tumor tissues through the enhanced permeability and retention (EPR) effect through blood circulation by passive targeting.[76] The growth state and density of vascular endothelial in the tumor area can also affect the EPR effect.[77] Active targeting nanoparticles, modified with the ligand, can enter into the cells through receptor-ligand-mediated endocytosis by recognizing specific receptors on the surface of tumor cells. They have stronger specificity and a significant effect to increase the intracellular drug concentration in tumor cells.[78]

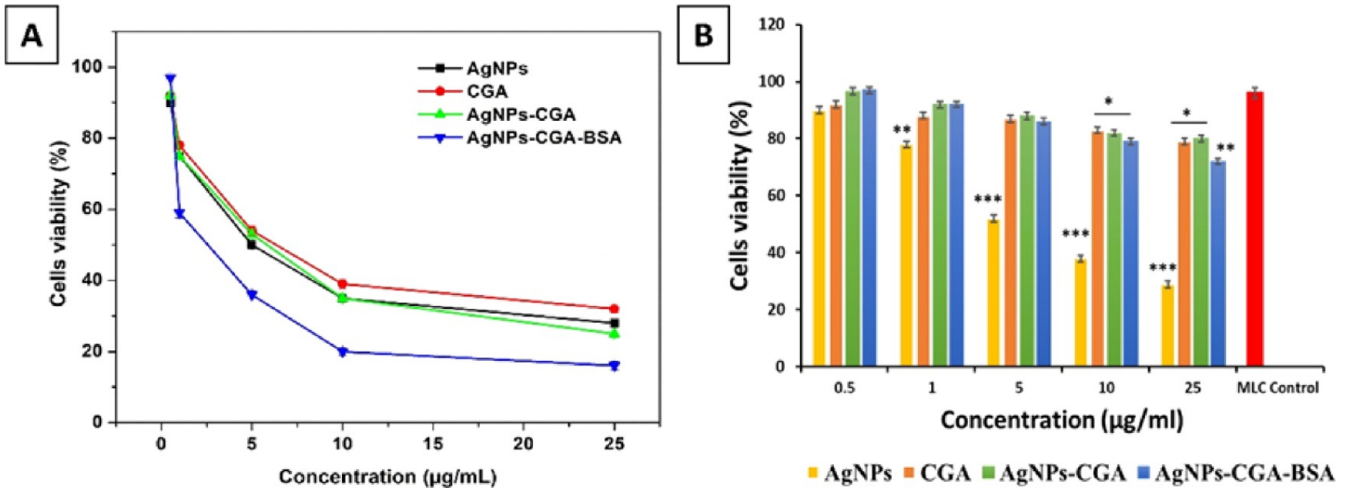

Figure 5. Cell viability study. The IC_{50} value of CGA and AgNPs-CGA-BSA for DLA cells were 6.29 and 2.5 μg/mL, respectively (A). Cell viability study in MLC cells in a concentration-dependent manner (B). Values were expressed as mean ± SEM of three different experiments. (*p < 0.05, **p < 0.01, and ***p < 0.001.)

https://doi.org/10.1021/acsomega.2c05989
ACS Omega 2022, 7, 48018−48033

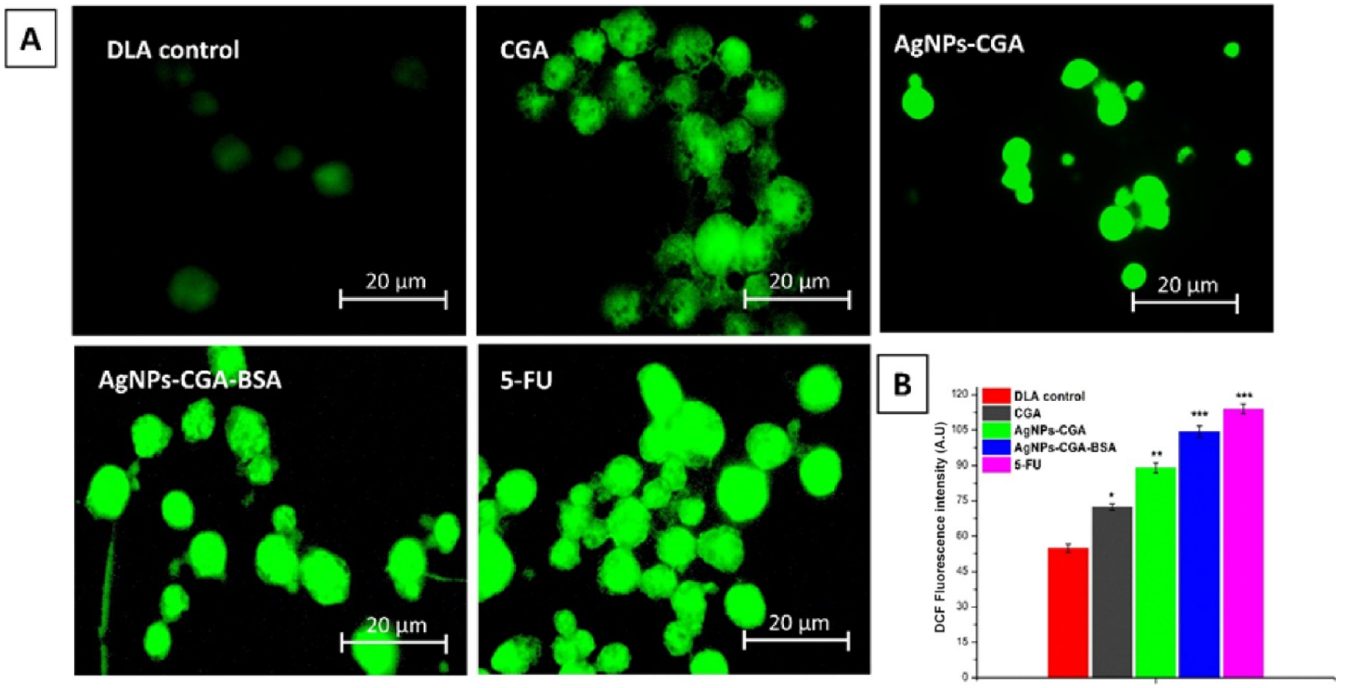

Figure 6. Study of intracellular ROS generation using H_2DCFDA (2′,7′-dichlorodihydrofluorescein diacetate) (A); the figure showed the DCF fluorescence intensity after the treatment with CGA, AgNPs-CGA, and AgNPs-CGA-BSA at their respective IC_{50} doses (B). Values were expressed as mean ± SEM of three different experiments (*p < 0.05, **p < 0.01, and ***p < 0.001).

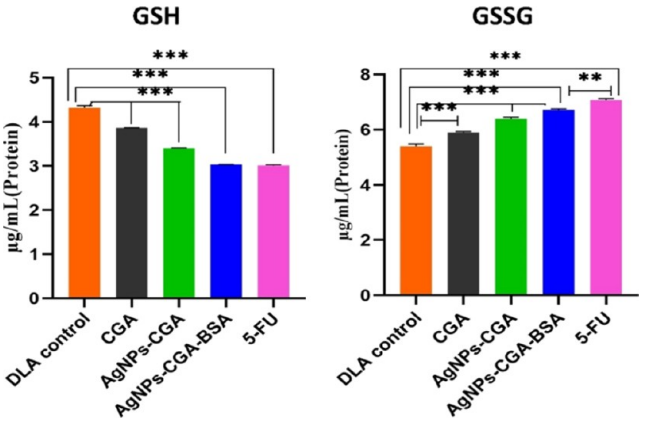

Figure 7. Intracellular GSH and oxidized glutathione (GSSG) levels in DLA cells. Values were expressed as mean ± SEM of three different experiments; **p < 0.01 and ***p < 0.001, compared with the DLA control.

3.4.4. Expression of Enzymatic Antioxidants (SOD and CAT) in DLA Cells. To evaluate the involvement of enzymatic antioxidants in the anticancer activity of AgNPs-CGA-BSA in DLA cells, the expression of SOD and CAT was measured by the western blot technique. The present study (Figure 8A,B) showed that expression of SOD and catalase in DLA cells was significantly reduced after the application of AgNPs-CGA-BSA which may be compared with the positive control 5-fluorouracil (5-FU).[49,50]

3.4.5. Apoptotic Changes in Nuclear Chromatin by DAPI and PI Staining. DAPI easily penetrates the dead cells and binds with the minor groove of dsDNA, and fluorescence increases by approximately 20-fold. PI stains fragmented chromatin of dsDNA in apoptotic cells by producing red color. AgNPs-CGA-BSA exhibited characteristic apoptotic morphology by showing cytoplasmic and nuclear shrinkage, chromatin condensation, and apoptotic bodies.[40] In the untreated DLA cells, the stained nuclei were more rounded and homogeneously stained with DAPI and PI than in the AgNPs-CGA- and AgNPs-CGA-BSA-treated cells, in which the appearance of crescents around the periphery of the nucleus or bright blue or bright red spherical beads was seen on the entire chromatin, which is a hallmark of early and late apoptosis (Figure 9).

3.5. In Vivo Anticancer Potential in DLA-Bearing Swiss Albino Mice. *3.5.1. Tumor Cell Count in DLA-Bearing Mice.* Reductions in tumor cell count in tumor hosts are a reliable criterion for the evaluation of the anticancer potential of an anticancer agent.[79] Results showed that AgNPs-CGA-BSA significantly reduced the tumor cell count in DLA-bearing mice compared to CGA and the control group (Figure 10). This effect of AgNPs-CGA-BSA proved its excellent anticancer potential against DLA cells. The percentage of cell count (CGA [69.16%], AgNPs-CGA [53.33%], AgNPs-CGA-BSA [37.5%], and 5-FU [34.16%]) was found in the AgNPs-CGA-BSA compared to other groups.

3.5.2. Hematological Study. Comparative analysis of the hematologic parameters in the AgNPs-CGA and AgNPs-CGA-BSA nanoparticle-treated mice and control animals is shown in Tables 1 and 2. RBC, WBC, and hemoglobin were decreased, and WBC count significantly augmented in the DLA-control group in comparison to the normal control group. Hb and RBC were significantly increased after the treatment of AgNPs-CGA-BSA, and the WBC count was significantly restored to about normal levels (Table 3).[80]

3.5.3. Histopathological Study. Histopathological analysis of the liver and kidney by H&E staining in DLA cells bearing Swiss albino mice after the treatment with CGA, AgNPs-CGA, and AgNPs-CGA-BSA was carried out. The results showed that in the saline control group, liver hepatocytes exhibited a

https://doi.org/10.1021/acsomega.2c05989
ACS Omega 2022, 7, 48018−48033

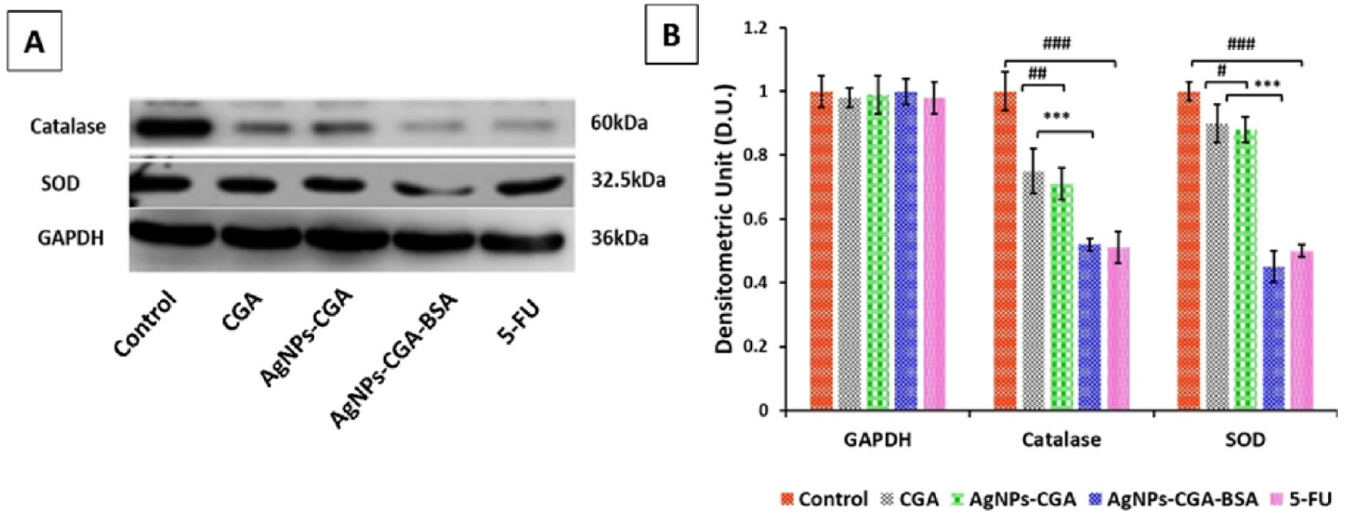

Figure 8. Oxidative stress and redox effect of catalase, SOD, and GAPDH gene expression in DLA cells by immunoblotting assay. Expressions of catalase and SOD were analyzed by the western blot using the corresponding antibodies. GAPDH was used as a control (A); a graphical representation of catalase and SOD, and results are expressed as mean ± SEM; ###$p < 0.001$, compared with the DLA control, and *$p < 0.05$, **$p < 0.01$, and ***$p < 0.001$, compared with CGA (B).

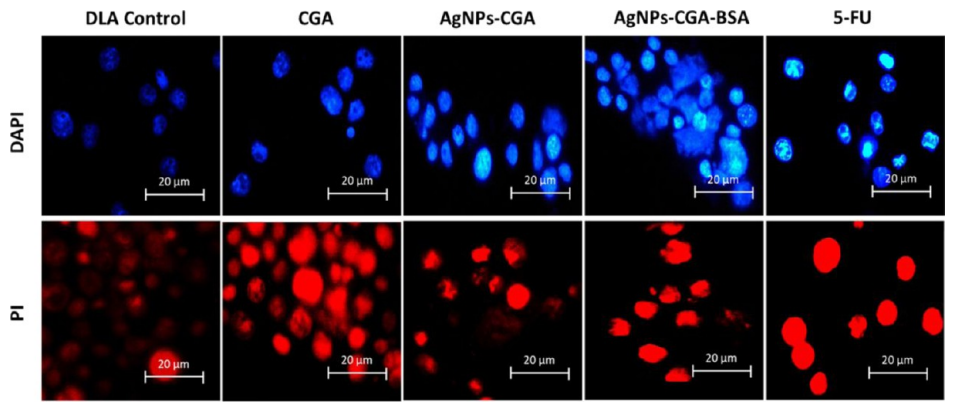

Figure 9. Chromatin condensation was studied by DAPI and PI staining in DLA cells. Cells were incubated with CGA, AgNPs-CGA, and AgNPs-CGA-BSA at their respective IC_{50} doses, and cells were stained with DAPI and PI. Images were taken with a fluorescence microscope.

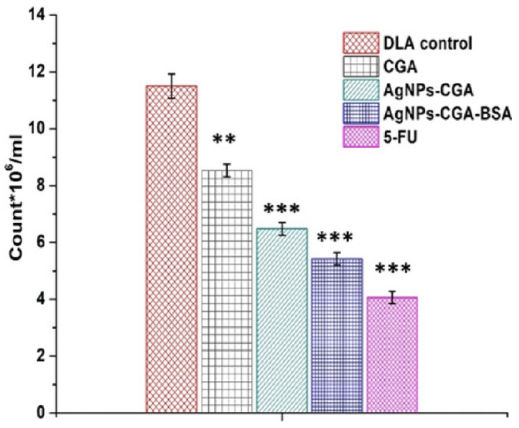

Figure 10. Effect of CGA, AgNPs-CGA, and AgNPs-CGA-BSA on tumor cell count. Values were expressed as mean ± SEM of three different experiments; **$p < 0.01$ and ***$p < 0.001$, compared with the DLA control.

typical hepatic architecture with hepatic tissues, portal structures, and blood sinusoids. After the treatment with CGA, AgNPs-CGA, and 5-FU, intense degenerative changes in the hepatocytes and renal tubules were observed (Figure 11). In the kidney, after the treatment with CGA, notable changes were observed in the renal tubular epithelial lining, renal corpuscle, and glomerulus including degranulated cytoplasm, pycnotic nuclei, congested blood vessels, and damaged glomerular. This result indicates severe hepatic and nephron toxicity induced by CGA and AgNPs-CGA. Interestingly, AgNPs-CGA-BSA remarkably restored the hepatic and renal architecture compared to the DLA control and CGA (Figure 12). This finding proved that BSA modification in AgNPs-CGA reduced its toxic effect and established AgNPs-CGA-BSA as a suitable anticancer agent with less toxicity.[81]

3.6. In Vivo Host Antioxidant Status in DLA-Bearing Swiss Albino Mice. *3.6.1. GSH Level.* A significant reduction in hepatic and renal GSH levels was observed in DLA control group animals. AgNPs-CGA-BSA brought back GSH levels to near-normal values in the mice's liver and kidney tissues (Figure 13). Liver and kidney GSH levels were found to be significantly ($p < 0.001$) higher compared to control group animals and almost similar to that of 5-FU-treated group animals.[82] Tumor progression markedly reduced cellular GSH, which may be due to oxidative stress.[83] Decreased levels of GSH might be a result of the effective conversion of GSH to

https://doi.org/10.1021/acsomega.2c05989
ACS Omega 2022, 7, 48018−48033

Table 2. Effect of AgNPs-CGA on Haematological Parameters of Swiss Albino Mice

hematological parameters	saline control	50 μg/kg bwt	100 μg/kg bwt	250 μg/kg bwt	500 μg/kg bwt	1000 μg/kg bwt	2000 μg/kg bwt
Hb percentage	15 ± 0.577	14.9 ± 0.5	14.8 ± 0.25	14.5 ± 0.41	14.3 ± 0.54	14 ± 0.32	13.2 ± 0.54*
total RBC count (mm^3)	6 ± 0.145	6 ± 0.012	5.8 ± 0.104	5.5 ± 0.05	5.2 ± 0.057	5 ± 0.01*	4.8 ± 0.02*
total WBC count (mm^3)	5100 ± 58	5100 ± 50	5200 ± 62	5300 ± 60	5400 ± 78	5500 ± 65*	5650 ± 50*

Table 3. Effect of AgNPs-CGA-BSA on Haematological Parameters of Swiss Albino Mice

hematological parameters	saline control	50 μg/kg bwt	100 μg/kg bwt	250 μg/kg bwt	500 μg/kg bwt	1000 μg/kg bwt	2000 μg/kg bwt
Hb percentage	15 ± 0.577	14.8 ± 0.25	14.8 ± 0.25	14.5 ± 0.4	14.5 ± 0.54	14.2 ± 0.32	14 ± 0.54*
total RBC count (mm^3)	6 ± 0.145	5.8 ± 0.104	5.8 ± 0.104	5.8 ± 0.05	5.5 ± 0.057	5.1 ± 0.04*	5.1 ± 0.02*
total WBC count (mm^3)	5100 ± 58	5100 ± 50	5200 ± 62	5300 ± 60	5300 ± 78	5300 ± 60*	5400 ± 50*

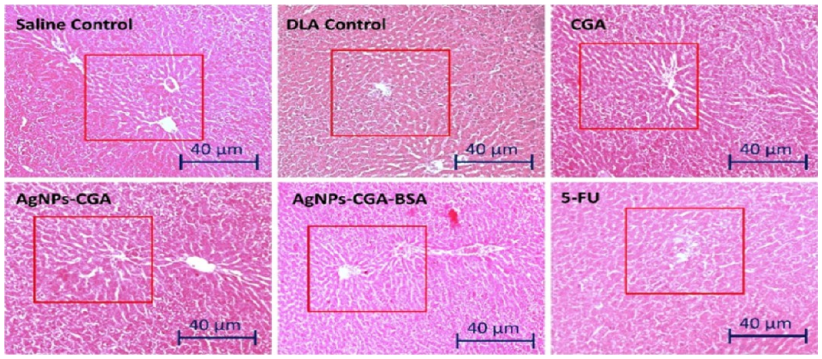

Figure 11. Histopathological study of the liver tissue of Swiss albino mice. The tissue section was stained with hematoxylin−eosin (H&E) and observed under a light microscope (scale bar: 40 μm) after the treatment with CGA, AgNPs-CGA, and AgNPs-CGA-BSA. 5-FU was used as a standard drug.

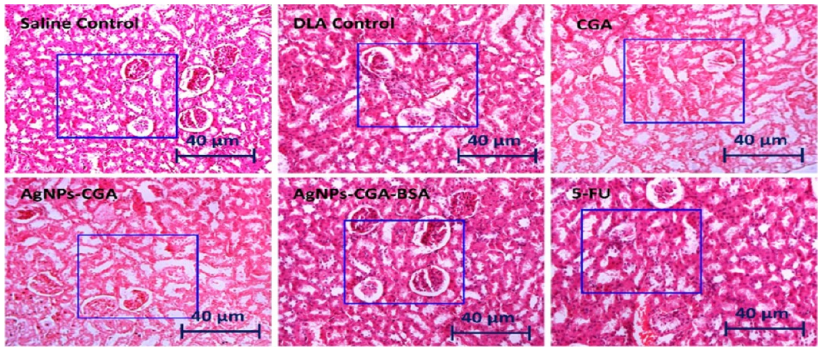

Figure 12. Histopathological study of the kidney tissue of Swiss albino mice. The tissue section was stained with hematoxylin−eosin (H&E) and observed under a light microscope (scale bar: 40 μm) after the treatment with CGA, AgNPs-CGA, and AgNPs-CGA-BSA. 5-FU was used as a standard drug.

GSSG by increased free radicals in tumor cells. Significant improvement in liver and kidney GSH was achieved by the treatment of AgNPs-CGA-BSA, signifying the protective role of AgNPs-CGA-BSA in DLA-bearing mice.

3.6.2. MDA Levels. Administration of AgNPs-CGA-BSA significantly decreased the MDA level in the liver and kidney of DLA-bearing mice. After treatment with AgNPs-CGA-BSA at the different dose levels, hepatic and renal MDA decreased significantly compared to the DLA control group (Figure 13). During oxidative degeneration of cancerous tissues, MDA, a free oxygen radical product, is formed.[84] It is the end product of lipid peroxidation and is an oxidative stress biomarker that has been reported to be displayed at greater levels in cancer tissues than in nondiseased organs.[85]

3.6.3. Catalase Level. The activity of catalase (CAT) was significantly decreased in the DLA control group compared to the saline control group. AgNPs-CGA-BSA increased hepatic and renal CAT activity significantly at dose levels of 2 and 4 mg/kg body wt (Figure 13). A similar finding was noted in our study in the case of 5-FU. As compared to normal tissues of the same origin, some authors described a catalase down-regulation,[86,87] indicating that cancer cells are frequently more sensitive to oxidative stress.[88]

3.6.4. SOD Level. The SOD level was decreased both in the liver and kidney of DLA control animals. The treatment with AgNPs-CGA-BSA at 2 and 4 mg/kg body wt doses reversed these changes to near-normal values in the liver and kidney of treated mice (Figure 13). An almost similar finding was observed in the case of 5-FU-treated mice. AgNPs-CGA-BSA at 4 mg/kg body wt dose level was found to be more effective to bring back the liver SOD's normal level. AgNPs-CGA-BSA at both doses normalized the SOD activity to a good extent

https://doi.org/10.1021/acsomega.2c05989
ACS Omega 2022, 7, 48018−48033

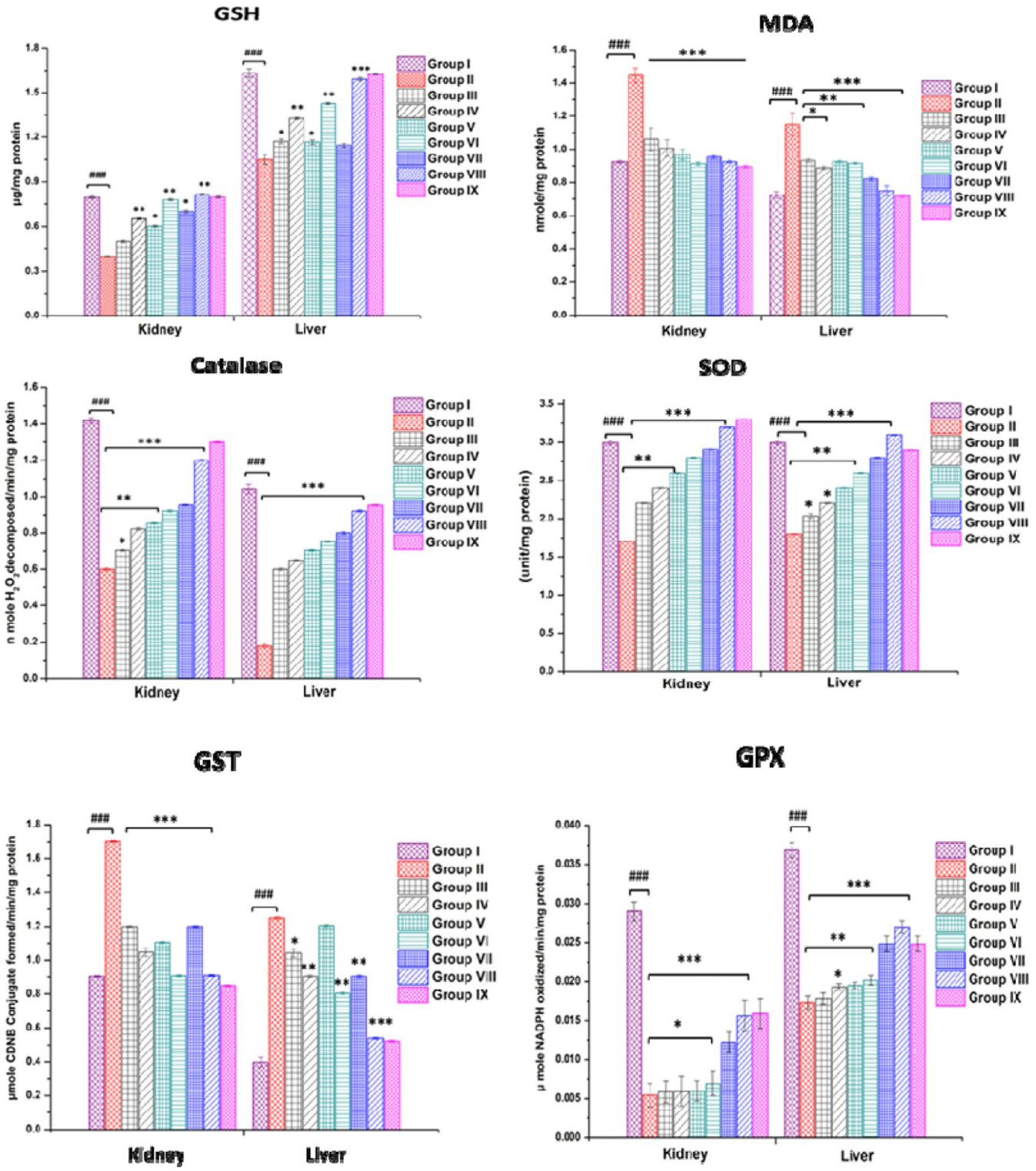

Figure 13. In vivo antioxidant status in DLA-bearing Swiss albino female mice. In vivo antioxidant activity of CGA, AgNPs-CGA, and AgNPs-CGA-BSA was studied in the kidney and liver tissues of DLA-bearing Swiss albino female mice. Results are expressed as mean ± SEM; $^{###}p < 0.001$, compared with the saline control, and $^{*}p < 0.05$, $^{**}p < 0.01$, and $^{***}p < 0.001$, compared with DLA control-bearing mice.

compared to the DLA control. The result is similar to the study.[89]

3.6.5. Glutathione-s-Transferase Level. A pronounced decrease in liver and kidney GST activity was also observed in DLA control animals.[90] The treatment with AgNPs-CGA-BSA at the abovementioned dose levels increased the GST level significantly to near-normal levels in treated groups (Figure 13).[91]

3.6.6. Glutathione Peroxidase Level. The activity of glutathione peroxidase (GPx) was significantly decreased in the liver and kidneys of DLA control animals compared to the saline control group. After treatment with AgNPs-CGA-BSA,

https://doi.org/10.1021/acsomega.2c05989
ACS Omega 2022, 7, 48018−48033

GPx activity increased significantly in the liver and kidney (Figure 13).[91]

4. CONCLUSIONS

This study has made an effort to look into the *in vitro* antioxidant and antineoplastic activity of AgNPs-CGA-BSA against Dalton's lymphoma ascites cells both *in vitro* and in vivo. AgNPs-CGA-BSA displayed *in vitro* antioxidant potential by showing DPPH and lipid peroxidase radical scavenging activity. AgNPs-CGA-BSA exhibits *in vitro* antineoplastic efficacy by triggering cytotoxicity, oxidative stress, and apoptotic chromatin condensation in DLA cells. At 2.5 μg/mL (IC_{50}), AgNPs-CGA-BSA showed selective cytotoxicity toward DLA cells while being non-toxic to MLC. AgNPs-CGA-BSA exhibits in vivo anticancer efficacy by uplifting the host antioxidant status by enhancing hepatic and renal GSH content and antioxidant enzymes in DLA bearing Swiss albino mice. This study throws light on the promising role of AgNPs-CGA-BSA as a therapeutic agent in the future for the treatment of oxidative stress-related disorders, especially cancer..

AUTHOR INFORMATION

Corresponding Author

Sujata Maiti Choudhury − *Biochemistry, Molecular Endocrinology and Reproductive Physiology Laboratory, Department of Human Physiology, Vidyasagar University, Midnapore 721102 West Bengal, India*; Email: sujata_vu@mail.vidyasagar.ac.in, sujata.vu2009@gmail.com

Authors

Tamanna Roy − *Biochemistry, Molecular Endocrinology and Reproductive Physiology Laboratory, Department of Human Physiology, Vidyasagar University, Midnapore 721102 West Bengal, India*

Surya Kanta Dey − *Biochemistry, Molecular Endocrinology and Reproductive Physiology Laboratory, Department of Human Physiology, Vidyasagar University, Midnapore 721102 West Bengal, India*

Ananya Pradhan − *Biochemistry, Molecular Endocrinology and Reproductive Physiology Laboratory, Department of Human Physiology, Vidyasagar University, Midnapore 721102 West Bengal, India*

Angsuman Das Chaudhuri − *Biochemistry, Molecular Endocrinology and Reproductive Physiology Laboratory, Department of Human Physiology, Vidyasagar University, Midnapore 721102 West Bengal, India*

Malay Dolai − *Department of Chemistry, Prabhat Kumar College, Purba Medinipur 721404 West Bengal, India*; orcid.org/0000-0001-7697-3376

Santi M. Mandal − *Central Research Facility, Indian Institute of Technology, Kharagpur 721302, India*; orcid.org/0000-0002-0119-7138

Complete contact information is available at: https://pubs.acs.org/10.1021/acsomega.2c05989

Notes

The authors declare no competing financial interest.

ACKNOWLEDGMENTS

The authors are grateful to Vidyasagar University, Midnapore (WB) for providing all the facilities to succeed in these studies. The authors sincerely acknowledge IIT-KGP for the instrumentation facilities to carry out some measurements.

REFERENCES

(1) Warraich, U.-e.-A.; Hussain, F.; Kayani, H. U. Aging-Oxidative stress, antioxidants and computational modeling. *Heliyon* **2020**, *6*, No. e04107.

(2) Nayyar, A.; Gindina, S.; Barron, A.; Hu, Y.; Danias, J. Do epigenetic changes caused by commensal microbiota contribute to development of ocular disease? A review of evidence. *Hum. Genomics* **2020**, *14*, 1−2.

(3) Lomeli, N.; Bota, D. A.; Davies, K. J. Diminished stress resistance and defective adaptive homeostasis in age-related diseases. *Clin. Sci.* **2017**, *131*, 2573−2599.

(4) Jozefczak, M.; Remans, T.; Vangronsveld, J.; Cuypers, A. Glutathione is a key player in metal-induced oxidative stress defenses. *Int. J. Mol. Sci.* **2012**, *13*, 3145−3175.

(5) Aquilano, K.; Baldelli, S.; Ciriolo, M. R. Glutathione: new roles in redox signaling for an old antioxidant. *Front. Pharmacol.* **2014**, *5*, 196.

(6) Tan, B. L.; Norhaizan, M. E.; Liew, W. P.; Sulaiman Rahman, H. Antioxidant and oxidative stress: a mutual interplay in age-related diseases. *Front. Pharmacol.* **2018**, *9*, 1162.

(7) Condello, M.; Meschini, S. Role of natural antioxidant products in colorectal cancer disease: a focus on a natural compound derived from prunusspinosa, trigno ecotype. *Cells* **2021**, *10*, 3326.

(8) Barbouti, A.; Lagopati, N.; Veroutis, D.; Goulas, V.; Evangelou, K.; Kanavaros, P.; Gorgoulis, V. G.; Galaris, D. Implication of dietary iron-chelating bioactive compounds in molecular mechanisms of oxidative stress-induced cell ageing. *Antioxidants* **2021**, *10*, 491.

(9) Winston, D.*Adaptogens: Herbs for Strength, Stamina, and Stress Relief*; Simon & Schuster Digital Sales Inc.: India, 2022.

(10) Alsayari, A.; Wahab, S. Genus Ziziphus for the treatment of chronic inflammatory diseases. *Saudi J. Biol. Sci.* **2021**, *28*, 6897−6914.

(11) Monirul Hasan Tipu, M. M.; Baroi, A.; Rana, J.; Islam, S.; Jahan, R.; Shipon Miah, M. S.; Asaduzzaman, M.Potential Applications of Nanotechnology in Agriculture: A Smart Tool for Sustainable Agriculture. *Agricultural Development in Asia-Potential Use of Nano-Materials and Nano-Technology*; Intech Open, 2021.

(12) Saavedra, M. J.; Aires, A.; Dias, C.; Almeida, J. A.; De Vasconcelos, M. C. B. M.; Rosa, P.; Rosa, E. A. Evaluation of the potential of squash pumpkin by-products (seeds and shell) as sources of antioxidant and bioactive compounds. *Food Sci. Technol.* **2015**, *52*, 1008−1015.

(13) Bharat Helkar, P. B.; Sahoo, A. K.; Patil, N. J. Review: Food industry by-products used as a functional food ingredients. *Int. J. Waste Resour.* **2016**, *6*, 1−6.

(14) Ahmed, R.; Hamed, R.; Ali, I. A.; Sedeek, S.; Abelyan, N. A.; Al-Sanea, M. Cancer Chemopreventive Potential and Chemical Profiling of Euphorbia abyssinica Endowed with Docking Studies. *ACS Omega* **2022**, *7*, 3596−3604.

(15) Hemlata, G. S.; Gupta, K. K.; Tejavath, K. K. ROS-Mediated Apoptosis Induced by BSA Nanospheres Encapsulated with Fruit Extract of Cucumis prophetarum in Various Human Cancer Cell Lines. *ACS Omega* **2021**, *6*, 10383−10395.

(16) de Martel, C.; Georges, D.; Bray, F.; Ferlay, J.; Clifford, G. M. Global burden of cancer attributable to infections in 2018: a worldwide incidence analysis. *Lancet Global Health* **2020**, *8*, 180−190.

(17) Yin, S. Y.; Yang, N. S.; Lin, T. J. Phytochemicals approach for developing cancer immunotherapeutics. *Front. Pharmacol.* **2017**, *8*, 386.

(18) Shahcheraghi, S. H.; Ayatollahi, J.; Lotfi, M.; Bafghi, A. F.; Khaleghinejad, S. H. Application of nano drugs in treatment of leishmaniasis. *Global J. Infect Dis. Clin. Res.* **2016**, *2*, 018−020.

(19) Lu, H.; Tian, Z.; Cui, Y.; Liu, Z.; Ma, X. Chlorogenic acid: A comprehensive review of the dietary sources, processing effects, bioavailability, beneficial properties, mechanisms of action, and future directions. *Compr. Rev. Food Sci. Food Saf.* **2020**, *19*, 3130−3158.

(20) Alcázar Magaña, A. A.; Kamimura, A.; Soumyanath, A.; Stevens, J. F.; Maier, C. S. Caffeoylquinic acids: Chemistry, biosynthesis, occurrence, analytical challenges, and bioactivity. *Plant J.* **2021**, *107*, 1299−1319.
(21) Marchiosi, R.; dos Santos, W. D.; Constantin, R. P.; de Lima, R. B.; Soares, A. R.; Finger-Teixeira, A.; Mota, T. R.; de Oliveira, D. M.; Foletto-Felipe, M. D.; Abrahão, J.; Ferrarese-Filho, O. Biosynthesis and metabolic actions of simple phenolic acids in plants. *Phytochem. Rev.* **2020**, *19*, 865−906.
(22) Hemlata; Meena, P. R.; Singh, A. P.; Tejavath, K. K. Biosynthesis of Silver Nanoparticles Using Cucumis prophetarum Aqueous Leaf Extract and Their Antibacterial and Antiproliferative Activity Against Cancer Cell Lines. *ACS Omega* **2020**, *5*, 5520−5528.
(23) Sood, R.; Chopra, D. S. Improved yield of green synthesized crystalline silver nanoparticles with potential antioxidant activity. *Int. Res. J. Pharm.* **2012**, *8*, 100−104.
(24) Mintz, K. J.; Leblanc, R. M. The use of nanotechnology to combat liver cancer: Progress and perspectives. *Biochim. Biophys. Acta, Rev. Cancer* **2021**, *1876*, 188621.
(25) Patra, J. K.; Das, G.; Fraceto, L. F.; Campos, E. V. R.; Rodriguez-Torres, M. D. P.; Acosta-Torres, L. S.; Diaz-Torres, L. A.; Grillo, R.; Swamy, M. K.; Sharma, S.; Habtemariam, S.; Shin, H.-S. Nano based drug delivery systems: recent developments and future prospects. *J. Nanobiotechnol.* **2018**, *16*, 71.
(26) Li, Z.; Ma, W.; Ali, I.; Zhao, H.; Wang, W.; Qiu, Q. Green and Facile Synthesis and Antioxidant and Antibacterial Evaluation of Dietary Myricetin-Mediated Silver Nanoparticles. *ACS Omega* **2020**, *5*, 32632−32640.
(27) Patra, J. K.; Das, G.; Kumar, A.; Ansari, A.; Kim, H.; Shin, H. S. Photo-mediated biosynthesis of silver nanoparticles using the non-edible accrescent fruiting calyx of Physalis peruviana L. fruits and investigation of its radical scavenging potential and cytotoxicity activities. *J. Photochem. Photobiol., B* **2018**, *188*, 116−125.
(28) Annu, S.; Ahmed, G.; Kaur, P.; Sharma, S.; Singh, S.; Ikram, S. Fruit waste (peel) as bio-reductant to synthesize silver nanoparticles with antimicrobial, antioxidant and cytotoxic activities. *J. Appl. Biomed.* **2018**, *16*, 221−231.
(29) Wang, W.; Wei, W. Green Fabrication of Bioactive Silver Nanoparticles Using Mentha pulegium Extract under Alkaline: An Enhanced Anticancer Activity. *ACS Omega* **2022**, *7*, 1494−1504.
(30) Hosny, H.; Eltaweil, S. E.; Mostafa, M.; El-Badry, A.; Hussein, E. E.; Omer, E. H.; Fawzy, M. O.; Manal, F. Facile Synthesis of Gold Nanoparticles for Anticancer, Antioxidant Applications, and Photocatalytic Degradation of Toxic Organic Pollutants. *ACS Omega* **2022**, *7*, 3121−3133.
(31) Das, G.; Patra, J. K.; Debnath, T.; Ansari, A.; Shin, H. S. Investigation of antioxidant, antibacterial, antidiabetic, and cytotoxicity potential of silver nanoparticles synthesized using the outer peel extract of Ananas comosus (L.). *PLoS One* **2019**, *14*, No. e0220950.
(32) Nosrati, H.; Salehiabar, M.; Manjili, H. K.; Danafar, H.; Davaran, S. Preparation of magnetic albumin nanoparticles via a simple and one-pot desolvation and co-precipitation method for medical and pharmaceutical applications. *Int. J. Biol. Macromol.* **2018**, *108*, 909−915.
(33) Nosrati, H.; Salehiabar, M.; Manjili, H. K.; Danafar, H.; Davaran, S. Preparation of magnetic albumin nanoparticles via a simple and one-pot desolvation and co-precipitation method for medical and pharmaceutical applications. *Int. J. Biol. Macromol.* **2018**, *108*, 909−915.
(34) Nosrati, H.; Sefidi, N.; Sharafi, A.; Danafar, H.; Kheiri Manjili, H. K. Bovine Serum Albumin (BSA) coated iron oxide magnetic nanoparticles as biocompatible carriers for curcumin-anticancer drug. *Bioorg. Chem.* **2018**, *76*, 501−509.
(35) Li, Y.; Xia, Y.; Liu, K.; Ye, K.; Wang, Q.; Zhang, S.; Huang, Y.; Liu, H. Constructing Fe-MOF-Derived Z Scheme Photocatalysts with Enhanced Charge Transport: Nanointerface and Carbon Sheath Synergistic Effect. *ACS Appl. Mater. Interfaces* **2020**, *12*, 25494−25502.
(36) Madhu, M.; Xue, Q. Y.; Tseng, W. B.; Chen, T. H.; Krishna Kumar, K. A.; Tseng, W. L. MoS2 and MoSe2 Nanosheets as Triggers for Glutathione Dimerization in Solution and Glutathione Oxidation in Live Cells. *ACS Appl. Nano Mater.* **2022**, *5*, 10583−10595.
(37) Al-Marhaby, F. A.; Seoudi, R. Preparation and characterization of silver nanoparticles and their use in catalytic reduction of 4-Nitrophenol. *World J. Nano Sci. Eng.* **2016**, *06*, 29.
(38) Premkumar, M. P.; Thiruvengadaravi, K. V.; Senthil Kumar, K. P.; Nandagopal, J.; Sivanesan, S.Eco-Friendly Treatment Strategies for Wastewater Containing Dyes and Heavy Metals. *Environmental Contaminants*; Springer: Singapore, 2018; pp 317−360.
(39) Khullar, P.; Singh, V.; Mahal, A.; Dave, P. N.; Thakur, S.; Kaur, G.; Singh, J.; Singh Kamboj, K. S.; Singh Bakshi, B. M. Bovine serum albumin bioconjugated gold nanoparticles: synthesis, hemolysis, and cytotoxicity toward cancer cell lines. *J. Phys. Chem. C* **2012**, *116*, 8834−8843.
(40) Pradhan, A.; Bepari, M.; Maity, P.; Roy, S. S.; Roy, S.; Choudhury, S. M. Gold nanoparticles from indole-3-carbinol exhibit cytotoxic, genotoxic and antineoplastic effects through the induction of apoptosis. *Sci. Rep.* **2016**, *6*, 56435−56449.
(41) Maity, P.; Bepari, M.; Pradhan, A.; Baral, R.; Roy, S.; Maiti Choudhury, S. M. Synthesis and characterization of biogenic metal nanoparticles and its cytotoxicity and anti-neoplasticity through the induction of oxidative stress, mitochondrial dysfunction and apoptosis. *Colloids Surf., B* **2018**, *161*, 111−120.
(42) Thiruvengadam, M.; Chung, I. M.; Gomathi, T.; Ansari, M. A.; Gopiesh Khanna, K. V.; Babu, V.; Rajakumar, G. Synthesis, characterization and pharmacological potential of green synthesized copper nanoparticles. *Bioprocess Biosyst. Eng.* **2019**, *42*, 1769−1777.
(43) Hawezy, H. J. S.; Sdiq, K. H.; Qadr, V. A.; Anwer, S. S.; Salih, S. J. Biosynthesis of magnetite-nanoparticles using microalgae (Spirulina sp. and Spirogyra sp.). *Plant Archives* **2020**, *20*, 1023−1027.
(44) Deepty, M.; Srinivas, C.; Kumar, E.; Mohan, N. K.; Prajapat, C. L.; Rao, T. C.; Meena, S. S.; Verma, A. K.; Sastry, D. L. XRD, EDX, FTIR and ESR spectroscopic studies of co-precipitated Mn−substituted Zn−ferrite nanoparticles. *Ceram. Int.* **2019**, *45*, 8037−8044.
(45) Hamouda, R. A.; Hussein, M. H.; Abo-elmagd, R. A.; Bawazir, S. S. Synthesis and biological characterization of silver nanoparticles derived from the cyanobacteriumOscillatorialimnetica. *Sci. Rep.* **2019**, *9*, 13071.
(46) Gaber, N. B.; El-Dahy, S. I.; Shalaby, E. A. Comparison of ABTS, DPPH, permanganate, and methylene blue assays for determining antioxidant potential of successive extracts from pomegranate and guava residues. *Biomass Convers. Biorefin.* **2021**, DOI: 10.1007/s13399-021-01386-0.
(47) Janarny, G.; Ranaweera, K. K.; Gunathilake, K. D. Antioxidant activities of hydro-methanolic extracts of Sri Lankan edible flowers. *Biocatal. Agric. Biotechnol.* **2021**, *35*, 102081.
(48) Choudhury, S. M.; Gupta, M.; Majumder, U. K. Antineoplastic activities of MT81 and its structural analogue in Ehrlich ascites carcinoma-bearing swiss albino mice. *Oxid. Med. Cell. Longevity* **2010**, *3*, 61−70.
(49) Xue, R.; Meng, Q.; Lu, D.; Liu, X.; Wang, Y.; Hao, J. Mitofusin2 induces cell autophagy of pancreatic cancer through inhibiting the PI3K/Akt/mTOR signaling pathway. *Oxid. Med. Cell. Longevity* **2018**, *2018*, 2798070.
(50) Saha, P.; Mazumder, U. K.; Haldar, P. K.; Naskar, S.; Kundu, S.; Bala, A.; Kar, B. Anticancer activity of methanol extract of Cucurbita maxima against Ehrlich ascites carcinoma. *International Journal of Research in Pharmaceutical Sciences* **2011**, *2*, 52.
(51) Tekin, S.; Seven, E. Assessment of serum catalase, reduced glutathione, and superoxide dismutase activities and malondialdehyde levels in keratoconus patients. *Eye* **2021**, *36*, 2062−2066.
(52) Daves, M.; Zagler, E. M.; Cemin, R.; Gnech, F.; Joos, A.; Platzgummer, S.; Lippi, G. Sample stability for complete blood cell count using the Sysmex XN haematological analyser. *Blood Transfus.* **2015**, *13*, 576−582.

https://doi.org/10.1021/acsomega.2c05989
ACS Omega 2022, 7, 48018−48033

(53) Standish, R. A.; Cholongitas, E.; Dhillon, A.; Burroughs, A. K.; Dhillon, A. P. An appraisal of the histopathological assessment of liver fibrosis. *Gut* **2006**, *55*, 569−578.
(54) Abd_al ameer, H. M.; Al-Mayali, W. M.; Kadhem, W. M. Evaluation of some antioxidants and malondialdehyde (MDA) in iraqi women infected with breast cancer and toxoplasmosis in Al-Diwaniyah and Al-Najaf provinces. *Mater. Today: Proc.* **2021**, DOI: 10.1016/j.matpr.2021.07.236.
(55) Wang, X.; Ma, A.; Yang, J. Genetic parameter estimates for three antioxidant factors in cultured Takifugurubripes. *Fish Shellfish Immunol.* **2021**, *119*, 645−650.
(56) Gusti, A. M.; Qusti, S. Y.; Alshammari, E. M.; Toraih, E. A.; Fawzy, M. S. Antioxidants-Related Superoxide Dismutase (SOD), Catalase (CAT), Glutathione Peroxidase (GPX), Glutathione-S-Transferase (GST), and Nitric Oxide Synthase (NOS) Gene Variants Analysis in an Obese Population: A Preliminary Case-Control Study. *Antioxidants* **2021**, *10*, 595.
(57) Pavlovschi, E.; Pantea, V.; Borovic, D.; Tagadiuc, O. Glutathione-related antioxidant defense system in patients with hypertensive retinopathy. *Rom. J. Ophthalmol.* **2021**, *65*, 46.
(58) Shao, F.; Yang, A.; Yu, D. M.; Wang, J.; Gong, X.; Tian, H. X. Bio-synthesis of Barleria gibsoni leaf extract mediated zinc oxide nanoparticles and their formulation gel for wound therapy in nursing care of infants and children. *J. Photochem. Photobiol., B* **2018**, *189*, 267−273.
(59) Zhang, L.; Liu, Y.; Wang, Y.; Xu, M.; Hu, X. UV−Vis spectroscopy combined with chemometric study on the interactions of three dietary flavonoids with copper ions. *Food Chem.* **2018**, *263*, 208−215.
(60) Sulaiman, G. M.; Hussien, H. T.; Saleem, M. M. Biosynthesis of silver nanoparticles synthesized by Aspergillus flavus and their antioxidant, antimicrobial and cytotoxicity properties. *Bull. Mater. Sci.* **2015**, *38*, 639−644.
(61) Hamouda, R. A.; Hussein, M. H.; Abo-elmagd, R. A.; Bawazir, S. S. Synthesis and biological characterization of silver nanoparticles derived from the cyanobacterium Oscillatorialimnetica. *Sci Rep.* **2019**, *9*, 1−7.
(62) Elumalai, M.; Vimalraj, S.; Chandirasekar, S.; Ezhumalai, N.; Kasthuri, J.; Rajendiran, N. N-Cholyl d-Penicilamine Micelles Templated Red Light-Emitting Silver Nanoclusters: Fluorometric Sensor for S2−Ions and Bioimaging Application Using Zebrafish Model. *Langmuir* **2022**, *38*, 7580.
(63) Madhu, M.; Tseng, W. L. NaCl nanocrystal-encapsulated carbon dots as a solution-based sensor for phosphorescent sensing of trace amounts of water in organic solvents. *Anal. Methods* **2021**, *13*, 4949−4954.
(64) Hsiao, M. C.; Liao, S. H.; Yen, M. Y.; Liu, P. I.; Pu, N. W.; Wang, C. A.; Ma, C. C. Preparation of covalently functionalized graphene using residual oxygen-containing functional groups. *ACS Appl. Mater. Interfaces* **2010**, *2*, 3092−3099.
(65) Huang, H.; Xia, L.; Shi, X.; Asiri, A. M.; Sun, X. Ag nanosheets for efficient electrocatalytic N 2 fixation to NH 3 under ambient conditions. *Chem. Commun.* **2018**, *54*, 11427−11430.
(66) Anand, K.; Kaviyarasu, K.; Muniyasamy, S.; Roopan, S. M.; Gengan, R. M.; Chuturgoon, A. A. Bio-Synthesis of Silver Nanoparticles Using Agroforestry Residue and Their Catalytic Degradation for Sustainable Waste Management. *J. Cluster Sci.* **2017**, *28*, 2279−2291.
(67) Mollick, M. M. R.; Rana, D.; Dash, S. K.; Chattopadhyay, S.; Bhowmick, B.; Maity, D.; Mondal, D.; Pattanayak, S.; Roy, S.; Chakraborty, M.; Chattopadhyay, D. Studies on Green Synthesized Silver Nanoparticles Using Abelmoschus Esculentus (L.) Pulp Extract Having Anticancer (in Vitro) and Antimicrobial Applications. *Arabian J. Chem.* **2019**, *12*, 2572−2584.
(68) Saha, P.; Mahiuddin, M.; Islam, A. N.; Ochiai, B. Biogenic synthesis and catalytic efficacy of silver nanoparticles based on peel extracts of citrus macroptera fruit. *ACS Omega* **2021**, *6*, 18260−18268.
(69) Zhang, Y.; Ji, L.; Qiu, W.; Shi, X.; Asiri, A. M.; Sun, X. Iodide-derived nanostructured silver promotes selective and efficient carbon dioxide conversion into carbon monoxide. *Chem. Commun.* **2018**, *54*, 2666−2669.
(70) Korshed, P.; Li, L.; Ngo, D. T.; Wang, T. Effect of Storage Conditions on the Long-Term Stability of Bactericidal Effects for Laser Generated Silver Nanoparticles. *Nanomaterials* **2018**, *8*, 218.
(71) Hazra, B.; Biswas, S.; Mandal, N. Antioxidant and free radical scavenging activity of Spondiaspinnata. *BMC Complementary Altern. Med.* **2008**, *8*, 1−10.
(72) Gangwar, M.; Gautam, M. K.; Sharma, A. K.; Tripathi, Y. B.; Goel, R. K.; Nath, G. Antioxidant capacity and radical scavenging effect of polyphenol rich Mallotus philippenensis fruit extract on human erythrocytes: an in vitro study. *Sci. World J.* **2014**, *2014*, 279451.
(73) Reitznerová, A.; Šuleková, M.; Nagy, J.; Marcinčák, S.; Semjon, B.; Čertík, M.; Klempová, T. Lipid peroxidation process in meat and meat products: A comparison study of malondialdehyde determination between modified 2-thiobarbituric acid spectrophotometric method and reverse-phase high-performance liquid chromatography. *Molecules* **2017**, *22*, 1988.
(74) Zandvakili, A.; Moradi, M.; Ashoo, P.; Pournejati, R.; Yosefi, R.; Karbalaei-Heidari, H. R.; Behaein, S. Investigating cytotoxicity effect of Ag-deposited, doped and coated titanium dioxide nanotubes on breast cancer cells. *Mater. Today Commun.* **2022**, *32*, 103915.
(75) Majeed, S.; Danish, M.; Zakariya, N. A.; Hashim, R.; Ansari, M. T.; Sisinthy, S. P. Tailored silver nanoparticles capped with gallic acid and its potential toxicity via ROS mediated pathway against osteosarcoma cells. *Mater. Today Commun.* **2022**, *32*, 103844.
(76) Bertrand, N.; Wu, J.; Xu, X.; Kamaly, N.; Farokhzad, O. C. Cancer Nanotechnology: The Impact of Passive and Active Targeting in the Era of Modern Cancer Biology. *Adv. Drug Delivery Rev.* **2014**, *66*, 2−25.
(77) Maeda, H. Toward a Full Understanding of the EPR Effect in Primary and Metastatic Tumors as Well as Issues Related to Its Heterogeneity. *Adv. Drug Delivery Rev.* **2015**, *91*, 3−6.
(78) Danhier, F.; Feron, O.; Préat, V. To Exploit the Tumor Microenvironment: Passive and Active Tumor Targeting of Nano-carriers for Anti-Cancer Drug Delivery. *J. Controlled Release* **2010**, *148*, 135−146.
(79) Kim, S. J.; Kim, H. S.; Seo, Y. R. Understanding of ROS-inducing strategy in anticancer therapy. *Oxid. Med. Cell. Longevity* **2019**, *2019*, 5381692.
(80) Rohini, K.; Surekha Bhat, B. M.; Srikumar, P. S.; Mahesh Kumar, K. A. Assessment of Hematological Parameters in Pulmonary Tuberculosis Patients. *Indian J. Clin. Biochem.* **2016**, *31*, 332−335.
(81) Ibrahim, K. E.; Al-Mutary, M. G.; Bakhiet, A. O.; Khan, H. A. Histopathology of the Liver, Kidney, and Spleen of Mice Exposed to Gold Nanoparticles. *Molecules* **2018**, *23*, 1848.
(82) Kavitha, C. N.; Raja, K. D.; Rao, S. K. Antitumor activity of Albizialebbeck L. against Ehrlich ascites carcinoma in vivo and HeLa and A549 cell lines in vitro. *J. Cancer Res. Ther.* **2021**, *17*, 491.
(83) Grăvilă, C.; Petrovici, S.; Stana, L.; Olariu, L.; Trif, A. Study on the blood glutathione protective effects induced during three rats generations by K2Cr2O7 intake. *J. Agroaliment. Processes Technol.* **2010**, *16*, 313−316.
(84) Gusti, A. M.; Qusti, S. Y.; Alshammari, E. M.; Toraih, E. A.; Fawzy, M. S. Antioxidants-Related Superoxide Dismutase (SOD), Catalase (CAT), Glutathione Peroxidase (GPX), Glutathione-S-Transferase (GST), and Nitric Oxide Synthase (NOS) Gene Variants Analysis in an Obese Population: A Preliminary Case-Control Study. *Antioxidants* **2021**, *10*, 595.
(85) Alam, B.; Majumder, R.; Akter, S.; Lee, S. H. Piper betle extracts exhibit antitumor activity by augmenting antioxidant potential. *Oncol. Lett.* **2014**, *9*, 863−868.
(86) Glorieux, C.; Zamocky, M.; Sandoval, J. M.; Verrax, J.; Calderon, P. B. Differential expression of manganese superoxide dismutase and catalase in lung cancer. *Cancer Res.* **2015**, *87*, 84−97.

(87) Cullen, J. J.; Mitros, F. A.; Oberley, L. W. Expression of antioxidant enzymes in diseases of the human pancreas: another link between chronic pancreatitis and pancreatic cancer. *Pancreas* **2003**, *26*, 23−27.
(88) Kwei, K. A.; Finch, J. S.; Thompson, E. J.; Bowden, G. T. Transcriptional repression of catalase in mouse skin tumor progression. *Neoplasia* **2004**, *6*, 440−448.
(89) Glorieux, C.; Calderon, P. B. Catalase, a remarkable enzyme: targeting the oldest antioxidant enzyme to find a new cancer treatment approach. *Biol. Chem.* **2017**, *398*, 1095−1108.
(90) Ozcelebi, H.; Ari, F.; Dere, E. Glutathione S-Transferase Activity in Tissues of Rats Exposed to Fenarimol. *Braz. Arch. Biol. Technol.* **2021**, *64*, No. e21200751.
(91) Alnomasy, A. E.; Albalawi, N. A.; Althobaiti, R. H.; Alhasani, S. F. Anti-tumor effects and cellular mechanisms of Pistacia atlantica methanolic extract against Ehrlich solid tumor in mice. *Asian Pac. J. Trop. Biomed.* **2022**, *12*, 69−77.

https://doi.org/10.1021/acsomega.2c05989
ACS Omega 2022, 7, 48018−48033